# Selective lymphodepletion underlies the efficacy of horse anti-thymocyte globulin-based immunosuppressive therapy in aplastic anemia

Emma S. Pool,[1] Cilia R. Pothast,[1] Shannah M. Gennesse,[1] Esther H.M. van Egmond,[1] Julia M. Giezen,[2] Sabrina A.J. Veld,[1] René E.M. Toes,[2] Frits Koning,[3] Constantijn J.M. Halkes,[1] Mirjam H.M. Heemskerk,[1] Dirk Jan A.R. Moes[4] and Jennifer M-L. Tjon[1]

[1]Department of Hematology; [2]Department of Rheumatology; [3]Department of Immunology and [4]Department of Clinical Pharmacy and Toxicology, Leiden University Medical Center, Leiden, the Netherlands

**Correspondence:** Jennifer M-L. Tjon
j.m.l.tjon@lumc.nl

**Received:** October 3, 2025.
**Accepted:** January 21, 2026.
**Early view:** January 29, 2026.

**https://doi.org/10.3324/haematol.2025.300002**

# Supplementary data

## Selective lymphodepletion underlies the efficacy of horse anti-thymocyte globulin-based immunosuppressive therapy in aplastic anemia

Emma S. Pool[1], Cilia R. Pothast[1], Shannah Gennesse[1], Esther H.M. van Egmond[1], Julia M. Giezen[2], Sabrina A.J. Veld[1], René E.M. Toes[2], Frits Koning[3], Constantijn J.M. Halkes[1], Mirjam H.M. Heemskerk[1], Dirk Jan A.R. Moes[4] and Jennifer M-L. Tjon[1]

[1] Department of Hematology, Leiden University Medical Center, Leiden, The Netherlands
[2] Department of Rheumatology, Leiden University Medical Center, Leiden, The Netherlands
[3] Department of Immunology, Leiden University Medical Center, Leiden, The Netherlands
[4] Department of Clinical Pharmacy and Toxicology, Leiden University Medical Center, Leiden, The Netherlands

## Supplementary methods

### Quantification of total ATGAM concentrations

Total ATGAM was defined as all horse IgG antibodies in the ATGAM preparation[1]. Total ATGAM concentrations in patient plasma were quantified by sandwich ELISA. 96-well plates were coated overnight at 4°C with goat anti-horse IgG antibodies at a dilution of 1:2500 in PBS (Jackson Immunoresearch, cat 108-005-003). Next, plates were blocked, washed using PBS with 0.005% Tween20, and incubated with diluted patient plasma samples for two hours at room temperature. Each sample was analyzed across eight serial dilutions. Subsequently, plates were washed five times using PBS with 0.005% Tween20 and incubated with a peroxidase-conjugated secondary goat anti-horse antibody at a dilution of 1:25,000. After a one hour incubation at room temperature, plates were washed five times using PBS with 0.005% Tween20 and stained with TMB substrate buffer for five minutes in the dark. Finally, staining was stopped and plates were measured at 450nm on a microplate photometer (ThermoFisher Multiskan FC). Total ATGAM concentrations in µg/mL in each plasma sample were calculated using the linear range of a standard curve, which was created by including serial dilutions of known ATGAM concentrations in each experiment.

### Quantification of active ATGAM concentrations

Active ATGAM was defined as the fraction of ATGAM that is capable of binding to human lymphocytes. To quantify active ATGAM concentrations in plasma, flow cytometry was performed based on a validated protocol for the quantification of alemtuzumab levels in patient plasma[2], which since has been optimized for the measurement of rabbit-derived anti-thymocyte globulin plasma concentrations[3]. Recent work shows this assay resulted in high-quality pharmacokinetic data for a cohort of 121 acute lymphoblastic leukemia patients who received rabbit-derived anti-thymocyte globulin as part of the conditioning regimen pre-HSCT[4]. In our study, first, cryopreserved PBMCs isolated from a healthy donor were thawed and plated in 96-well plates. PBMCs from the same donor were used in all experiments to enable comparisons between experiments. Subsequently, cells were incubated with non-diluted and 3x, 9x, and 27x diluted patient plasma for 30 minutes at 4°C. Afterwards, cells were washed twice in PBS and incubated with an AlexaFluor 488-conjugated goat anti-horse antibody diluted at 1:100 in a volume of 10µL for 30 minutes at 4°C (Jackson Immunoresearch, cat 108-545-003). Next, cells were washed twice in PBS and stained with a panel of six fluorochrome-conjugated antibodies in a volume of 10µL to distinguish all major immune lineages. The following antibodies were used: APC-H7 anti-human CD3 antibody diluted at 1:60 (BD Biosciences, cat 641406); PE-Cy7 anti-human CD4 antibody diluted at 1:3000 (Beckman Coulter, cat 6607101); Pacific Blue anti-human CD8 antibody diluted at 1:2000 (BioLegend, cat 301026); PerCP anti-human CD14 antibody diluted at 1:50 (BD Biosciences, cat 563372); APC anti-human CD19 antibody diluted at 1:50 (BD Biosciences, cat 555415) and BV510 anti-human CD56 antibody at 1:50 (BD Biosciences, cat 563041). After a 30 minute incubation at 4°C, cells were washed and measured immediately on the BD LSRFortessa™ cell analyzer (BD Biosciences). Data were analyzed in FlowJo (BD Biosciences) or OMIQ (Dotmatics). The gating strategy presented **Figure S1** determined the geometric mean fluorescence intensity of AlexaFluor 488-stained total lymphocytes, $CD4^+$ T-cells, $CD8^+$ T-cells, B-cells, NK-cells and monocytes in each acquired sample. Concentrations of ATGAM capable of binding to all

lymphocytes (active ATGAM), $CD4^+$ T-cells ($CD4^+$ T-cell-binding active ATGAM), $CD8^+$ T-cells ($CD8^+$ T-cell-binding active ATGAM), $CD19^+$ B-cells (B-cell-binding active ATGAM) and $CD56^+$ NK-cells (NK-cell-binding active ATGAM) were then calculated using the mean of two reference curves, which were created by exposing the PBMCs to known concentrations of ATGAM in each experiment. To ensure consistency between experiments, the reference curves were aliquoted and stored at -20°C to enable their use across experiments. Active ATGAM concentrations were calculated in arbitrary units (AU), and the concentration of 1mg/mL ATGAM was arbitrarily set as 1000 AU/mL. The lower limit of quantification (LLoQ) of the assay was 0.02 AU/mL. At high ATGAM concentrations of >200 AU/mL in patient plasma, accurate gating of NK-cells could not be performed. As a result, concentrations of NK-cell-binding active ATGAM were not determined on days 3 and/or 4 after the first ATGAM dose for a few patients. To confirm the robustness of the assay, we analyzed the duplicate measurement of undiluted patient plasma included in each experiment, and evaluated duplicate measurements of serial dilutions of ATGAM. This revealed strong correlations between technical duplicates ($p<0.001$), underscoring within-experiment reproducibility (**Figure S2A**). To confirm reproducibility between experiments, plasma samples collected from several AA patients pre- and post-ATGAM were measured in duplicate in independent experiments, which resulted in highly comparable results (**Figure S2B**).

**Population pharmacokinetic modelling and estimation of ATGAM exposure**

To estimate the full concentration *versus* time profile of total and active ATGAM, non-linear mixed-effects modeling was performed using the acquired total or active ATGAM concentration-time data. Model development was performed in NONMEM version 7.4.4 (Icon Development Solutions, Ellicott City, MD). Pirana version 2.9.8 (Certara, Princeton, NJ) was used as a modeling platform, while R version 4.4.1 ran in RStudio version 2023.03 was used for data visualization. Pharmacokinetic parameters were estimated using a first-order conditional estimation with interaction approach (FOCE+I). To identify the model with the best fit for the concentration-time data, both one- and two-compartment models, incorporating linear, non-linear or parallel linear and non-linear elimination, were evaluated. Inter-individual variability (IIV) in parameter estimates was evaluated using an exponential error model, while residual unexplained variability was characterized by testing additive, proportional and combined error models. Inter-occasion variability was examined for all pharmacokinetic parameters to determine whether pharmacokinetics varied between different ATGAM infusions. A detailed overview of the steps taken during model development is shown in **Tables S2** and **S3**.

To find the model that best described the concentration-time data, we compared each candidate model using the objective function value (OFV; -2 log likelihood). A lower OFV indicated a better fit, and a model was considered to have a significantly improved fit if its OFV decreased by at least 6.63 ($p\leq0.01$; based on 1 degree of freedom, and assuming a chi-square distribution). Models were also assessed visually using goodness-of-fit (GOF) plots. These plots compared observed (measured) ATGAM concentrations against both individual predicted (IPRED) and population predicted (PRED) ATGAM concentrations to assess how well the model captured the measured concentration-time data. Other GOF plots compared conditional weighted residuals (CWRES) against time or PRED. The aim of these plots was

to identify any systematic differences between the predicted and observed (measured) ATGAM concentrations. Other considerations in model selection included model pharmacokinetic parameter stability, inter-individual variability (IIV) and shrinkage, to ensure the model was well structured and not too complex for the available data.

To better understand the differences in the concentration-time profile of ATGAM between patients and to improve the predictive power of the model, we studied the influence of clinical covariates on the population pharmacokinetics of ATGAM. Potential covariates were selected based on physiological plausibility, and included age, sex and body weight. The effect of the selected covariates on ATGAM pharmacokinetics was initially evaluated visually, by examining how clearance (CL) or volume of distribution (V) were influenced by these covariates across all patients. Eta CL and V *versus* covariate plots were used. Given that ATGAM includes antibodies that can bind lymphocytes, we also assessed whether CL or V were influenced by differences in lymphocyte count pre-ATGAM between patients.

The final population pharmacokinetic models for total or active ATGAM were validated using prediction-corrected visual predictive checks (pcVPC)[5]. This approach relied on running the model 500 times to simulate new datasets, which were then compared to the observed (measured) ATGAM concentrations to confirm the performance of the model in predicting the ATGAM concentrations between patients. In addition, non-parametric bootstraps with 1000 simulations were performed to evaluate the precision of the final parameter estimates.

To estimate the full concentration *versus* time curve of the active ATGAM fractions capable of binding to $CD4^+$ T-cells, $CD8^+$ T-cells, B cells or NK cells, we ran the final population pharmacokinetic model (posthoc estimation) for active ATGAM using the concentration *versus* time data of each of these active ATGAM fractions.

To enable correlation analyses between ATGAM exposure and clinical parameters, we used the final population pharmacokinetic models that best described the concentration *versus* time data for total or active ATGAM to estimate individual pharmacokinetic parameters. These estimates were then used to calculate patients' cumulative exposure to total or active ATGAM, which was defined as the area under the concentration *versus* time curve ($AUC_{0\text{-}inf}$).

**Immune reconstitution data**

To correct for missing immune reconstitution data, we performed non-linear mixed effect modeling using the SAEMIX package[6] in R version 4.4.1. We used exponential models to predict total lymphocyte, $CD4^+$ T-cell, $CD8^+$ T-cell and NK-cell counts on each day between days 4 and 40 after start of ATGAM infusion in each patient. These models considered both the general trend across all patients and inter-individual differences. Predictions were only made for patients who had at least one measurement available between days 4 and 40 following infusion (n=43 patients), and are presented in **Figure S5**. B-cell reconstitution was not modeled using SAEMIX since no consistent trends were observed in the B-cell count-time data shortly after ATGAM administration between patients.

**Spectral flow cytometry data acquisition and analysis**

For deep immunophenotyping both before and at various time points after start of IST, spectral flow cytometry was performed. A 25-marker panel was designed to immunophenotype all major lymphoid lineages and to examine the binding of ATGAM to in-depth phenotyped immune cell subpopulations (**Table S1**). Cryopreserved PBMC samples from 3 AA patients, collected at AA diagnosis and up to 3.5 years after ATGAM infusion were studied (patients UPN13, UPN15 and UPN31; 7-10 samples per patient). All patients had very severe AA (VSAA), received four consecutive days 40 mg/kg/day ATGAM, responded to IST and were CMV seropositive at time of AA diagnosis. As a reference, cryopreserved PBMC samples from 5 age-, sex- and CMV status-matched healthy donors were studied. PBMC samples were thawed, plated into 96-well plates and rested at 37°C overnight. The next morning, cells were stained for viability with Zombie-NIR. Subsequently, cells were washed and stained with AlexaFluor 488-conjugated goat anti-horse IgG (Jackson Immunoresearch) diluted at 1:100 in a volume of 10µL for 30 minutes at room temperature to detect ATGAM-bound cells. Next, cells were washed and stained for 7 of 25 markers of the panel extracellularly in a volume of 10µL. This included BUV615-, PE- or APC-conjugated peptide-HLA tetramers, which were produced in-house and were added to evaluate the presence of CMV- and EBV-specific $CD8^+$ T-cells over time. After a 30 minute incubation at room temperature, cells were washed, fixed and stained intracellularly for the remaining 17 markers of the flow cytometry panel using the FoxP3/Transcription Factor Staining Buffer Set (Invitrogen; cat 00-5523-00) according to the manufacturer's instructions. As many markers as possible were stained intracellularly to avoid potential issues in detecting key cell surface markers, which could theoretically be masked for detection by the binding of ATGAM to these cell surface markers *in vivo*. Cells were then measured on the Aurora spectral flow cytometer (Cytek Biosciences). For each acquired flow cytometry data file, single, live lymphocytes were gated in OMIQ as shown in **Figure S3**. A median of $0.3 \cdot 10^6$ (range $0.02\text{-}0.5 \cdot 10^6$) single, live lymphocytes were gated for each sample, resulting in a dataset of $9.3 \cdot 10^6$ cells. To compare the cellular composition between samples, $0.1 \cdot 10^6$ cells were selected from each sample by downsampling, and visualized by performing UMAP dimensionality reduction analyses in OMIQ based on 15 neighbors, a minimum distance of 0.3 and 400 epochs. Only for the day 5 sample from patient UPN13 less cells were available ($0.02 \cdot 10^6$ cells), due lymphodepletion caused by ATGAM infusion. CD3, CD19 and anti-horse IgG stainings were not used generate the UMAP due to differences in marker expression intensities between samples. To distinguish all major lymphoid lineages, all single, live lymphocytes were clustered into 150 cell clusters using FlowSOM[7] in OMIQ, which were then merged to 6 clusters based on similarities in marker expression. Major lymphoid lineages were defined as follows: $CD3^+CD4^+$ T-cells, $CD3^+CD8^+$ T-cells, $CD3^+TCR\gamma\delta^+$ T-cells, $FoxP3^+$ regulatory T-cells, $CD3^-CD56^+$ NK-cells and $CD19^+$ B-cells. Analyses at the subpopulation level were performed by manual gating in OMIQ. R version 4.4.1 ran in RStudio version 2023.03 was used for data visualization and analysis.

For detailed characterization of $CD27^+$ B-cells post-ATGAM, cryopreserved PBMCs collected from UPN31 on day 13 after the first ATGAM infusion were stained with a 16-marker spectral flow cytometry antibody panel directed against B-cell surface markers. This panel enabled analysis of B-cell isotype distribution, activation status and expression of complement inhibitors. The panel also incorporated PE- and APC-conjugated tetanus toxoid to allow for

the detection of tetanus-specific B-cells. Cryopreserved PBMC samples from two sex- and age-matched healthy donors (also included in the larger spectral flow cytometry analysis) were included as a reference. Cells were fixed prior to acquisition on the Aurora spectral flow cytometer. Single, live B-cells were gated using the forward and side scatter, and by selecting $CD19^+$ B-cells while excluding all cells positive for the live dead stain. $0.2 \cdot 10^6$ cells single, live B-cells were gated from the day 13 sample from UPN31, while $0.5 \cdot 10^6$ and $1.1 \cdot 10^6$ single, live B-cells were acquired for the controls.

**Table S1.** Spectral flow cytometry panel for phenotyping of all lymphoid lineages.

| Marker | Fluorochrome | Clone | Manufacturer | Dilution | Extracellular / intracellular staining |
|---|---|---|---|---|---|
| CD45RA | BUV395 | HI100 | BD | 600 | Intracellular |
| CCR7 | BUV563 | 3D12 | BD | 100 | Extracellular |
| Tetramers CMV | BUV615 | NA | In-house | 75 | Extracellular |
| Tetramers EBV | BUV615 | NA | In-house | 75 | Extracellular |
| CD19 | BV421 | HIB19 | BioLegend | 160 | Intracellular |
| CD56 | BV510 | NCAM16.2 | BD | 30 | Intracellular |
| CD27 | BV570 | O323 | BioLegend | 30 | Extracellular |
| CD38 | BV605 | HIT2 | BD | 75 | Intracellular |
| CCR6 | BV711 | G034E3 | BioLegend | 40 | Extracellular |
| TCRγδ | BV750 | 11F2 | BD | 75 | Extracellular |
| CD24 | BV786 | ML5 | BioLegend | 100 | Intracellular |
| Goat anti-horse IgG | AF488 | NA | Jackson Immunoresearch | 100 | Extracellular |
| CD3 | RB545 | UCHT1 | BD | 1000 | Intracellular |
| FoxP3 | RB744 | 259D/C7 | BD | 75 | Intracellular |
| CD69 | RB780 | FN50 | BD | 2000 | Intracellular |
| IgD | PE | IADB6 | Beckman Coulter | 1000 | Extracellular |
| Tetramers EBV | PE | NA | In-house | 100 | Extracellular |
| Granzyme B | PE-CF594 | GB11 | BD | 1500 | Intracellular |
| CD28 | PE-Cy5 | CD28.2 | BD | 200 | Intracellular |
| CD8 | PE-fire 700 | SK1 | BioLegend | 1000 | Intracellular |
| Ki-67 | PE-Cy7 | B56 | BD | 400 | Intracellular |
| CD4 | PE-fire 810 | SK3 | BD | 800 | Intracellular |
| IgM | APC | MHM-88 | BioLegend | 160 | Intracellular |
| Tetramers CMV | APC | NA | In-house | 50 | Extracellular |
| KLRG1 | Spark NIR 685 | SA231A2 | BioLegend | 50 | Intracellular |
| HLA-DR | AF700 | G46-6 | BD | 75 | Intracellular |
| Live/dead | Zombie-NIR | NA | BioLegend | 500 | NA |
| Perforin | APC-fire 750 | B-D48 | BioLegend | 300 | Intracellular |

**Table S2**. Model building process for active ATGAM.

| Model number | Description | Model | Compared against | OFV | ΔOFV | Comments |
|---|---|---|---|---|---|---|
| 1 | One-compartment with linear elimination | CL = Θ1 × EXP(IIV)<br>V= Θ2 × EXP(IIV) | - | 84.063 | - | Additive error fixed to 0.0001 (rounding errors without fixation) |
| 2 | One-compartment with parallel linear and non-linear elimination | CL = Θ1 × EXP(IIV)<br>V= Θ2 × EXP(IIV)<br>Vmax= Θ3 × EXP(IIV)<br>Km= Θ4 × EXP(IIV) | 1 | 84.063 | 0 | Additive error fixed to 0.0001 |
| 3 | Two-compartment with linear elimination | CL = Θ1 × EXP(IIV)<br>Vc = Θ2 × EXP(IIV)<br>Q = Θ3 × EXP(IIV)<br>Vp = Θ4 | 2 | 57.611 | -26.45 | Additive error fixed to 0.0001 |
| 4 | Two-compartment with linear elimination + IIV V2 | CL = Θ1 × EXP(IIV)<br>Vc = Θ2 × EXP(IIV)<br>Q = Θ3 × EXP(IIV)<br>Vp = Θ4 × EXP(IIV) | 3 | -12.41 | -70.02 | Additive error fixed to 0.0001<br>Worse VPC (see **Figure S4**) |
| 4 | Two-compartment with linear elimination + OMEGA BLOCK between IIV CL and V1 | CL = Θ1 × EXP(IIV)<br>Vc = Θ2 × EXP(IIV)<br>Q = Θ3 × EXP(IIV)<br>Vp = Θ4 | 3 | 44.027 | -13.58 | Additive error fixed to 0.0001 |
| 5 | Two-compartment with linear elimination + OMEGA BLOCK between IIV CL and V1 + different proportional error ≥60AU/mL and <60AU/mL | CL = Θ1 × EXP(IIV)<br>Vc = Θ2 × EXP(IIV)<br>Q = Θ3 × EXP(IIV)<br>Vp = Θ4 | 4 | 34.705 | -9.322 | **Final model**<br>Additive error fixed to 0.0001<br>IIV CL: 43.1%<br>IIV Vc: 52%<br>IIV Q: 143.2% |
| 6 | Two-compartment with linear elimination + OMEGA BLOCK between IIV CL and V1 + different proportional error ≥60AU/mL and <60AU/mL + bodyweight as covariate | CL = Θ1 × EXP(IIV) × ((WT/MWT)**Θ5)<br>Vc = Θ2 × EXP(IIV) × ((WT/MWT)**Θ6)<br>Q = Θ3 × EXP(IIV)<br>Vp = Θ4 | 5 | 35.505 | 0.8 | Additive error fixed to 0.0001<br>IIV CL: 45.2%<br>IIV Vc: 50.8%<br>IIV Q: 145.9% |
| 7 | Two-compartment with linear elimination + OMEGA BLOCK between IIV CL and V1 + different proportional error ≥60AU/mL and <60AU/mL + lymphocyte count pre-ATGAM as covariate | CL = Θ1 × EXP(IIV) × (1+(LYMPH/MLYMPH)*Θ5)<br>Vc = Θ2 × EXP(IIV)<br>Q = Θ3 × EXP(IIV)<br>Vp = Θ4 | 5 | 36.813 | 2.108 | Additive error fixed to 0.0001<br>IIV CL: 42.9%<br>IIV Vc: 50.7%<br>IIV Q: 144.2% |
| 8 | Two-compartment with parallel linear and non-linear elimination | CL = Θ1 × EXP(IIV)<br>Vc= Θ2 × EXP(IIV)<br>Vp= Θ3<br>Vmax= Θ4 × EXP(IIV)<br>Km= Θ5 × EXP(IIV) | - | Model unstable | Model unstable | Additive error fixed to 0.0001 |

CL indicates clearance; IIV: inter-individual variability; Km: Michaelis-Menten contant; LYMPH: lymphocyte count pre-ATGAM; MLYMPH: median lymphocyte count pre-ATGAM; MWT: median population weight; OFV: objective function value; Q: intercompartmental clearance; V: volume of distribution; Vc: volume of distribution central compartment; Vp: volume of distribution peripheral compartment; Vmax: maximum elimination rate; WT: bodyweight.

**Table S3**. Model building process for total ATGAM.

| Model number | Description | Model | Compared against | OFV | ΔOFV | Comments |
|---|---|---|---|---|---|---|
| 1 | One-compartment with linear elimination | CL = Θ1 × EXP(IIV)<br>V= Θ2 × EXP(IIV) | - | 2026.3 | - | Additive error fixed to 0.0001 (rounding errors without fixation) |
| 2 | One-compartment with parallel linear and non-linear elimination | CL = Θ1 × EXP(IIV)<br>V= Θ2 × EXP(IIV)<br>Vmax= Θ3 × EXP(IIV)<br>Km= Θ4 × EXP(IIV) | 1 | 2026.4 | 0.06 | Additive error fixed to 0.0001. Model instable. |
| 3 | Two-compartment with linear elimination | CL = Θ1 × EXP(IIV)<br>Vc = Θ2 × EXP(IIV)<br>Q = Θ3 × EXP(IIV)<br>Vp = Θ4 | 1 | 1937.99 | -88.32 | Additive error fixed to 0.0001<br>Model unstable |
| 4 | Two-compartment with linear elimination + Vp fixed | CL = Θ1 × EXP(IIV)<br>Vc = Θ2 × EXP(IIV)<br>Vp = Θ4 FIX | 3 | 1940.7 | 2.72 | **Final model**<br>Additive error fixed to 0.0001<br>IIV CL: 44.0%<br>IIV Vc: 57.2%<br>IIV Q: 290.0% |
| 5 | Two-compartment with linear elimination + Vp fixed + OMEGA BLOCK between IIV CL and V1 | CL = Θ1 × EXP(IIV)<br>Vc = Θ2 × EXP(IIV)<br>Q = Θ3 × EXP(IIV)<br>Vp = Θ4 FIX | 4 | 1935.9 | -4.79 | Additive error fixed to 0.0001<br>IIV CL: 44.2%<br>IIV Vc: 58.1%<br>IIV Q: 303.3% |
| 6 | Two-compartment with linear elimination + Vp fixed + bodyweight as covariate | CL = Θ1 × EXP(IIV) × ((WT/MWT)**Θ5)<br>Vc = Θ2 × EXP(IIV) × ((WT/MWT)**Θ6)<br>Q = Θ3 × EXP(IIV)<br>Vp = Θ4 | 4 | 1947.2 | 6.48 | Additive error fixed to 0.0001<br>IIV CL: 50.5%<br>IIV Vc: 59.9%<br>IIV Q: 295.8% |
| 8 | Two-compartment with parallel linear and non-linear elimination | CL = Θ1 × EXP(IIV)<br>Vc= Θ2 × EXP(IIV)<br>Vp= Θ3<br>Vmax= Θ4 × EXP(IIV)<br>Km= Θ5 × EXP(IIV) | - | Model unstable | Model unstable | Additive error fixed to 0.0001 |

CL indicates clearance; IIV: inter-individual variability; Km: Michaelis-Menten contant; MWT: median population weight; OFV: objective function value; Q: intercompartmental clearance; V: volume of distribution; Vc: volume of distribution central compartment; Vp: volume of distribution peripheral compartment; Vmax: maximum elimination rate; WT: bodyweight.

**Table S4.** Model estimates for active ATGAM pharmacokinetic parameters.

| Parameter | Median (range) | Mean | RSE (%) | Shrinkage | 1000 bootstrap run results | |
|---|---|---|---|---|---|---|
| | | | | | Median | 95% CI |
| Clearance (CL in L/day) | 6.5 (3.4-24.0) | 6.97 | 11% | | 7.02 | 5.07 - 9.80 |
| Volume of distribution of central compartment ($V_c$ in L) | 1.5 (0.6-4.2) | 1.51 | 17% | | 1.51 | 0.88 - 2.86 |
| Intercompartmental clearance (Q in L/day) | 2.3 (0.5-65.2) | 3.2 | 38% | | 3.32 | 1.32 - 9.18 |
| Volume of distribution of peripheral compartment ($V_p$ in L) | 11.3 | 11.2 | 12% | | 11.56 | 6.51 - 22.94 |
| Inter-individual variability (IIV) | | | | | | |
| Clearance (IIV CL, %) | | 43.1 | 13% | 9% | 41.98 | 31.01 - 53.62 |
| CL ~ $V_c$ (%) | | - | - | - | 39.26 | 15.72 - 56.14 |
| Volume of distribution of central compartment (IIV Vc, %) | | 52 | 16% | 22% | 49.48 | 28.36 - 68.12 |
| Intercompartmental clearance (IIV Q, %) | | 143.2 | 17% | 8% | 141.75 | 102.51 - 194.50 |
| Random residual variability | | | | | | |
| Proportional error (CV%) | | 0.3 | 12% | | 0.30 | 0.23 - 0.57 |
| Additional error (AU/mL) | | 0.0001 | fixed | | 0.0001 | 0.0001 - 0.0001 |
| Half-life distribution phase (days) | 0.09 (0.02-0.25) | | | | | |
| Half-life elimination phase (days) | 4.5 (0.5-16.1) | | | | | |
| Peak concentration ($C_{max}$ in AU/mL) | 668.1 (208.6-1595.9) | | | | | |
| Total exposure ($AUC_{0-inf}$) | 1801.2 (583.9-4218.7) | | | | | |

**Table S5.** Model estimates for total ATGAM pharmacokinetic parameters.

| Parameter | Median (range) | Mean | RSE (%) | Shrinkage | 1000 bootstrap run results | |
|---|---|---|---|---|---|---|
| | | | | | Median | 95% CI |
| Clearance (CL in L/day) | 0.4 (0.2-1.4) | 0.426 | 8% | | 0.42 | 0.36 - 0.50 |
| Volume of distribution of central compartment ($V_c$ in L) | 3.3 (0.9-8.7) | 3.22 | 8% | | 3.17 | 2.65 - 3.67 |
| Intercompartmental clearance (Q in L/day) | 0.1 (0.0006-2.7) | 0.032 | 12% | | 0.03 | 0.01 - 0.15 |
| Volume of distribution of peripheral compartment ($V_p$ in L) | 0.9 | 0.949 | fixed | | 0.95 | 0.95 - 0.95 |
| Inter-individual variability (IIV) | | | | | | |
| Clearance (IIV CL, %) | | 44 | 14% | 10% | 43.10 | 28.65 - 55.37 |
| Volume of distribution of central compartment (IIV Vc, %) | | 57.2 | 10% | 4% | 57.10 | 46.13 - 69.76 |
| Intercompartmental clearance (IIV Q, %) | | 290 | 17% | 41% | 276.86 | 137.16 - 402.10 |
| Random residual variability | | | | | | |
| Proportional error (CV%) | | 0.355 | 10% | | 0.35 | 0.28 - 0.42 |
| Additional error (ug/mL) | | 0.0001 | fixed | | 0.0001 | 0.0001 - 0.0001 |
| Half-life distribution phase (days) | 4.3 (0.2-8.9) | | | | | |
| Half-life elimination phase (days) | 16.8 (1.8-1015.9) | | | | | |
| Peak concentration ($C_{max}$ in µg/mL) | 2500.7 (1175.4-7649.0) | | | | | |
| Total exposure ($AUC_{0\text{-}inf}$) | 28160.5 (9761.4-90999.0) | | | | | |

**Table S6.** Patient characteristics by active ATGAM exposure groups.

| Characteristic | Low active ATGAM exposure (n=15) | Medium active ATGAM exposure (n=14) | High active ATGAM exposure (n=15) | P-value |
|---|---|---|---|---|
| Age at diagnosis (median in years) | 40 | 60 | 57 | 0.21 |
| Sex (n) | | | | 0.32 |
| Male | 7 | 8 | 11 | |
| Female | 8 | 6 | 4 | |
| Disease severity at diagnosis (n) | | | | 0.91 |
| Non-severe AA | 2 | 3 | 2 | |
| Severe AA | 7 | 7 | 9 | |
| Very severe AA | 6 | 4 | 4 | |
| Weight at diagnosis (median in kg) | 71 | 75 | 88 | 0.003 |
| Height (median in cm) | 170 | 173 | 180 | 0.003 |
| Body mass index at diagnosis (median) | 22.4 | 24.5 | 26.0 | 0.33 |
| Neutrophils pre-ATGAM (median in $10^9$/L) | 0.33 | 0.24 | 0.31 | >0.9 |
| Reticulocytes pre-ATGAM (median in $10^9$/L) | 17.5 | 8.4 | 10 | 0.6 |
| Lymphocytes pre-ATGAM (median in $10^6$/L)[a] | 1625 | 1485 | 1315 | 0.75 |
| Eltrombopag added to IST (n) | 5 | 3 | 8 | 0.11 |
| Eltrombopag added with start ATGAM | 3 | 2 | 2 | |
| Eltrombopag added 20-180 days post-ATGAM | 2:<br>Day 96<br>Day 100 | 1:<br>Day 92 | 7:<br>Day 69<br>Day 86<br>Day 138<br>Day 160<br>Day 163<br>Day 165 | |
| Other second-line treatment ≤180 days post-ATGAM | 0 | 0 | 0 | 1.0 |
| Ciclosporin discontinued ≤180 days post-ATGAM | 0 | 0 | 1 | 0.40 |
| Deaths ≤180 days post-ATGAM | 2 | 1 | 1 | 0.78 |

[a]Data missing for 2 AA patients (1 in low and 1 in high exposure groups). Statistical differences between continuous variables calculated by Kruskal Wallis test. Statistical differences between categorical variables calculated by Fisher's Exact test. Statistical differences in addition of eltrombopag to IST, ciclosporin discontinuation and death calculated by log-rank (survival) test.

**Final active ATGAM pharmacokinetic model code**

```
$PROBLEM PK

$INPUT ID TIME DV TAD ATGNR C AMT RATE MDV EVID WEIGHT HEIGHT LYMPHO
CD4 CD8 NK B MONO dose_code ATGMgKg DaysATG ATGMgKgDay DayATGStart AGE
GENDER RESPONSE_3M RESPONSE_6M BMI

$DATA PK_ATGAM_data_ACTIVE.csv  IGNORE=@

$SUBROUTINES ADVAN6 TOL=3

$MODEL
COMP=(CENTRAL DEFOBS DEFDOSE)
COMP=(PERIPH)
COMP= AUC

$PK
CL = THETA(1) * EXP(ETA(1))
V1 = THETA(2) * EXP(ETA(2))
Q  = THETA(3) * EXP(ETA(3))
V2 = THETA(4)
S1 = V1
K10=CL/V1
K12=Q/V1
K21=Q/V2

$DES
C1=A(1)/V1
DADT(1)=-K10*A(1)-K12*A(1)+K21*A(2)
DADT(2)=-K21*A(2)+K12*A(1)
DADT(3)= C1

$ERROR
IPRED = F
IF(DV.GE.60) W = SQRT(THETA(5)**2*IPRED**2 + THETA(6)**2)
IF(DV.LT.60) W = SQRT(THETA(7)**2*IPRED**2 + THETA(6)**2)
   Y = IPRED + W*EPS(1)
 IRES = DV-IPRED
IWRES = IRES/W
AUC = A(3)
AUCCL = AMT/CL

$THETA
(0, 6.97) ; CL
(0, 1.51) ; V1
(0, 3.2) ; Q
(0, 11.2) ; V2
(0, 0.3) ; Prop.RE (sd)
(0.0001) FIX ; Add.RE (sd)
(0, 0.579) ; Prop.RE (sd)
```

```
$OMEGA BLOCK(2)
 0.186  ; IIV CL
 0.18 0.27  ; IIV V1
$OMEGA
 2.05 ; IIV Q

$SIGMA
 1 FIX  ; Proportional error PK

$EST METHOD=1 INTER MAXEVAL=2000 NOABORT SIG=2 PRINT=1 POSTHOC
$COV

; Xpose
$TABLE CL V1 V2 Q ID TIME DV MDV EVID PRED IPRED IWRES CWRES ETA1 ETA2
ETA3 LYMPHO CD4 CD8 B NK MONO AGE GENDER WEIGHT HEIGHT BMI AUCCL AUC
Response_3M Response_6M ONEHEADER NOPRINT FILE=sdtab002.3aa
$TABLE CL V1 ID TIME DV MDV EVID PRED IPRED IWRES CWRES ETA1 ETA2 ETA3
LYMPHO CD4 CD8 B NK MONO AGE GENDER WEIGHT HEIGHT AUCCL AUC
Response_3M Response_6M ONEHEADER NOPRINT FIRSTONLY FILE=patab002.3aa
```

**Final total ATGAM pharmacokinetic model code**

```
$PROBLEM PK

$INPUT ID TIME DV TAD ATGNR C AMT RATE MDV EVID WEIGHT HEIGHT LYMPH CD4
CD8 NK B MONO dose_code ATGMgKg DaysATG ATGMgKgDay DayATGStart AGE
GENDER RESPONSE_3M RESPONSE_6M

$DATA PK_ATGAM_data_TOTAL.csv  IGNORE=@

$SUBROUTINES ADVAN6 TOL=3

$MODEL
COMP=(CENTRAL DEFOBS DEFDOSE)
COMP=(PERIPH)
COMP= AUC

$PK
TVCL = THETA(1)
CL = TVCL * EXP(ETA(1))

TVV1 = THETA(2)
V1 = TVV1 * EXP(ETA(2))

TVQ = THETA(3)
Q  = TVQ * EXP(ETA(3))

TVV2 = THETA(4)
V2 = TVV2

S1 = V1

K10=CL/V1
K12=Q/V1
K21=Q/V2

$DES
C1=A(1)/V1
DADT(1)=-K10*A(1)-K12*A(1)+K21*A(2)
DADT(2)=-K21*A(2)+K12*A(1)
DADT(3)= C1

$ERROR
IPRED = F
   W = SQRT(THETA(5)**2*IPRED**2 + THETA(6)**2)
   Y = IPRED + W*EPS(1)
 IRES = DV-IPRED
IWRES = IRES/W
AUC = A(3)
AUCCL = AMT/CL
```

```
$THETA
(0, 0.424) ; CL
(0, 3.23) ; V1
(0, 0.0299) ; Q
(0.949) FIX ; V2
(0, 0.353) ; Prop.RE (sd)
(0.00001) FIX ; Add.RE (sd)

$OMEGA
 0.194 ; IIV CL
 0.318 ; IIV V1
 8.74 ; IIV Q

$SIGMA
 1 FIX  ; Proportional error PK

$EST METHOD=1 INTER MAXEVAL=2000 NOABORT SIG=2 PRINT=1 POSTHOC
$COV

; Xpose
$TABLE CL V1 V2 Q ID TIME DV MDV EVID PRED IPRED IWRES CWRES ETA1 ETA2
ETA3 LYMPH CD4 CD8 B NK MONO AGE GENDER WEIGHT HEIGHT AUCCL AUC
Response_3M Response_6M ONEHEADER NOPRINT FILE=sdtab005.3.2b3
$TABLE CL V1 V2 Q ETA1 ETA2 ETA3 LYMPH CD4 CD8 B NK MONO AGE GENDER
WEIGHT HEIGHT ONEHEADER NOPRINT FIRSTONLY FILE=patab005.3.2b3
```

## References


1. Regan JF, Lyonnais C, Campbell K, Smith LV, Buelow R, Group USTM-CS. Total and active thymoglobulin levels: effects of dose and sensitization on serum concentrations. Transpl Immunol. 2001;9(1):29-36.
2. Rebello P, Hale G. Pharmacokinetics of CAMPATH-1H: assay development and validation. J Immunol Methods. 2002;260(1-2):285-302.
3. Jol-van der Zijde CM, Bredius RG, Jansen-Hoogendijk AM, et al. IgG antibodies to ATG early after pediatric hematopoietic SCT increase the risk of acute GVHD. Bone Marrow Transplant. 2012;47(3):360-368.
4. Oostenbrink LVE, Von Asmuth EGJ, Jol-van der Zijde CM, et al. Anti-T-lymphocyte globulin exposure is associated with acute graft-versus-host disease and relapse in pediatric acute lymphoblastic leukemia patients undergoing hematopoietic stem cell transplantation: a multinational prospective study. Haematologica. 2024;109(9):2854-2863.
5. Bergstrand M, Hooker AC, Wallin JE, Karlsson MO. Prediction-corrected visual predictive checks for diagnosing nonlinear mixed-effects models. AAPS J. 2011;13(2):143-151.
6. Comets E, Lavenu A, Lavielle M. Parameter Estimation in Nonlinear Mixed Effect Models Using saemix, an R Implementation of the SAEM Algorithm. J Stat Softw. 2017;80(3):1-41.
7. Van Gassen S, Callebaut B, Van Helden MJ, et al. FlowSOM: Using self-organizing maps for visualization and interpretation of cytometry data. Cytometry A. 2015;87(7):636-645.

**Figure S1**

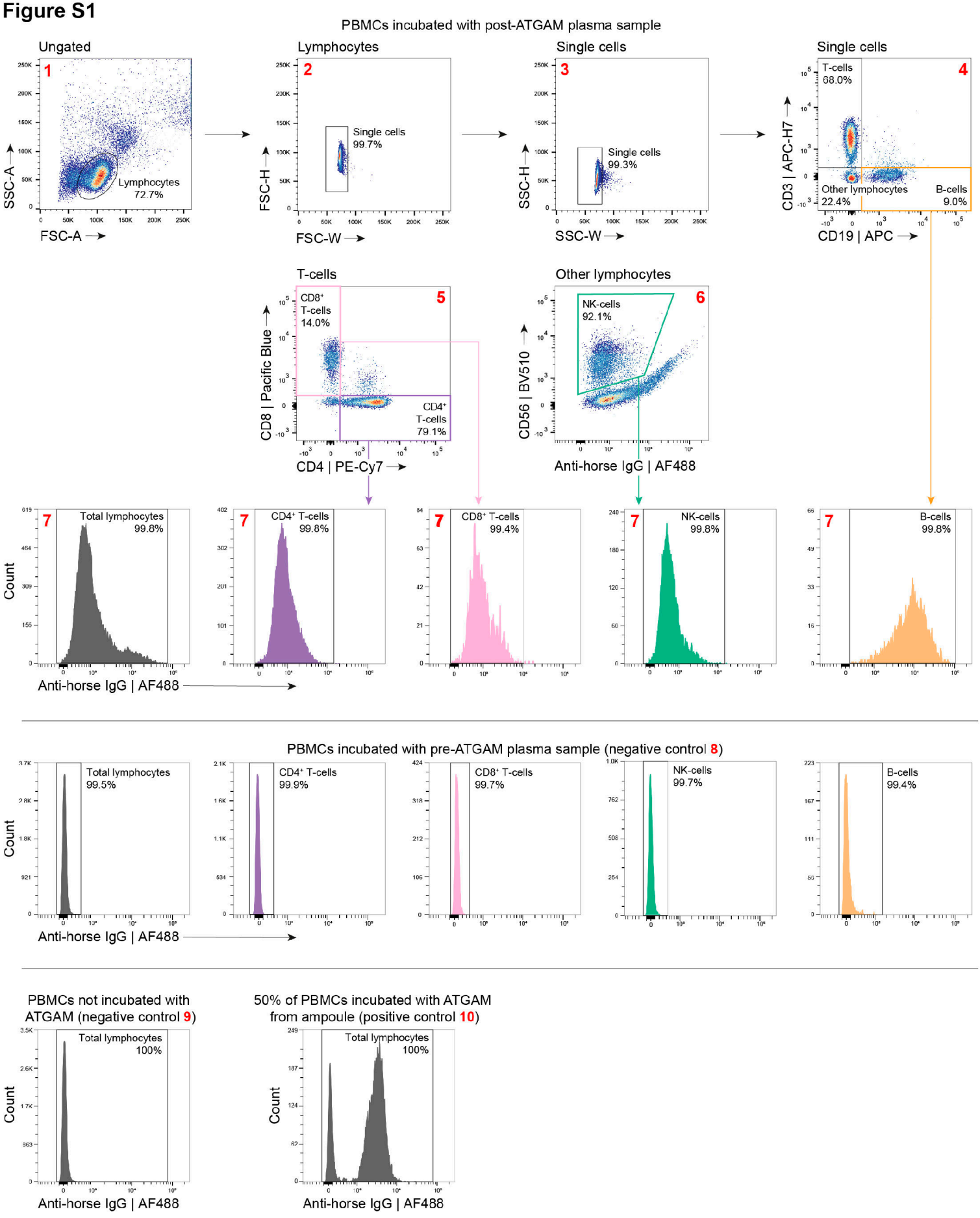
PBMCs incubated with post-ATGAM plasma sample
Ungated
1
SSC-A
FSC-A
Lymphocytes
72.7%
Lymphocytes
2
FSC-H
FSC-W
Single cells
99.7%
Single cells
3
SSC-H
SSC-W
Single cells
99.3%
Single cells
4
CD3 | APC-H7
CD19 | APC
T-cells
68.0%
Other lymphocytes
22.4%
B-cells
9.0%
T-cells
5
CD8 | Pacific Blue
CD4 | PE-Cy7
CD8⁺ T-cells
14.0%
CD4⁺ T-cells
79.1%
Other lymphocytes
6
CD56 | BV510
Anti-horse IgG | AF488
NK-cells
92.1%
7
Total lymphocytes
99.8%
CD4⁺ T-cells
99.8%
CD8⁺ T-cells
99.4%
NK-cells
99.8%
B-cells
99.8%
Count
Anti-horse IgG | AF488
PBMCs incubated with pre-ATGAM plasma sample (negative control 8)
Total lymphocytes
99.5%
CD4⁺ T-cells
99.9%
CD8⁺ T-cells
99.7%
NK-cells
99.7%
B-cells
99.4%
PBMCs not incubated with ATGAM (negative control 9)
Total lymphocytes
100%
50% of PBMCs incubated with ATGAM from ampoule (positive control 10)
Total lymphocytes
100%

**Figure S1. Gating strategy for quantification of active ATGAM plasma concentrations.** Lymphocytes were gated using the forward and side scatter (panel 1). Doublets were excluded, and single lymphocytes were selected for further analysis (panels 2-3). Within the single lymphocytes, $CD3^+$ T-cells, $CD19^+$ B-cells or $CD3^-CD19^-$ other lymphocytes were identified (panel 4). $CD4^+$ T-cells and $CD8^+$ T-cells were identified within the T-cell gate (panel 5). $CD56^+$ NK-cells were identified within the 'other lymphocyte' gate (panel 6). The geometric mean fluorescence intensity for the Alexa Fluor 488 anti-horse IgG antibody was determined for each gated population (panels 7). This was used to calculate the active ATGAM concentrations in the patient plasma sample using a reference curve obtained by exposing PBMCs to known concentrations of ATGAM. The gating strategy is shown for PBMCs incubated with a representative post-ATGAM patient plasma sample. Negative controls were included in each experiment and included PBMCs incubated with pre-ATGAM patient plasma samples (panels 8) and PBMCs not exposed to ATGAM (panel 9). Positive controls were PBMCs exposed to known concentrations of ATGAM (panel 10).

## Figure S2

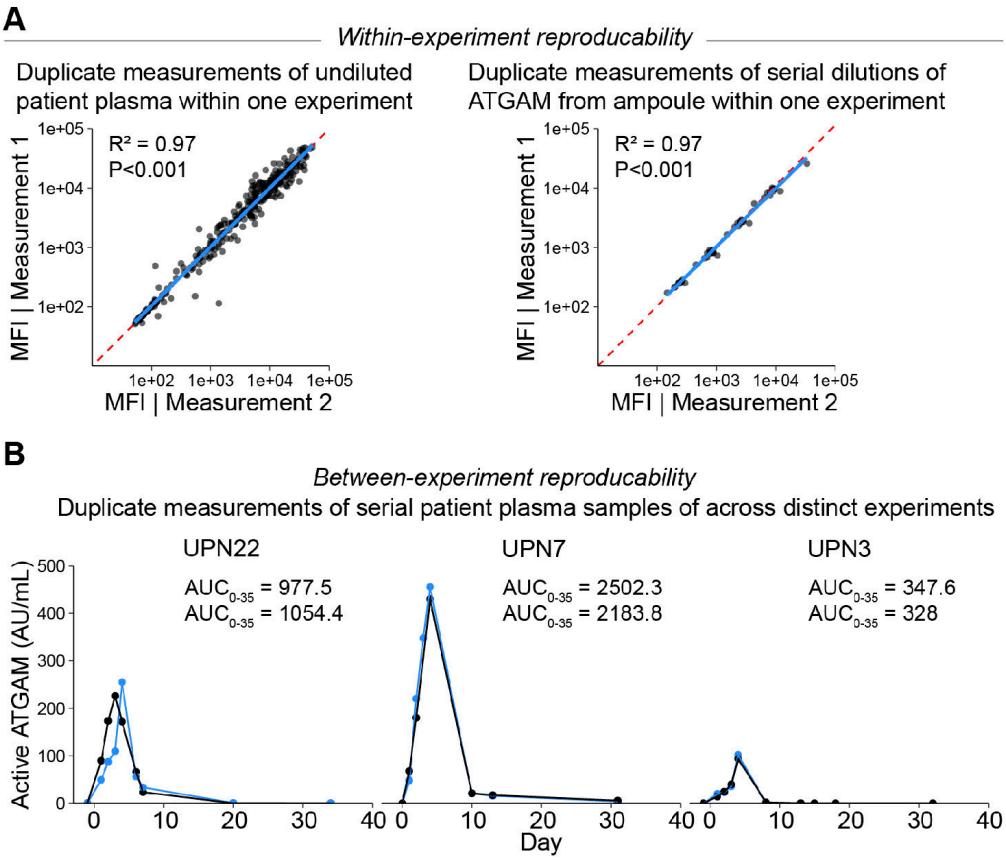


**Figure S2. Reproducability and robustness of the active ATGAM assay. [A]** Within-experiment reproducability, shown by correlation plot of duplicate measurements of undiluted patient plasma within a single experiment (left), or duplicate measurements of serial dilutions of ATGAM (right). **[B]** Between-experiment reproducability, shown by duplicate measurements of active ATGAM concentrations in patient plasma in independent experiments.

**Figure S3**

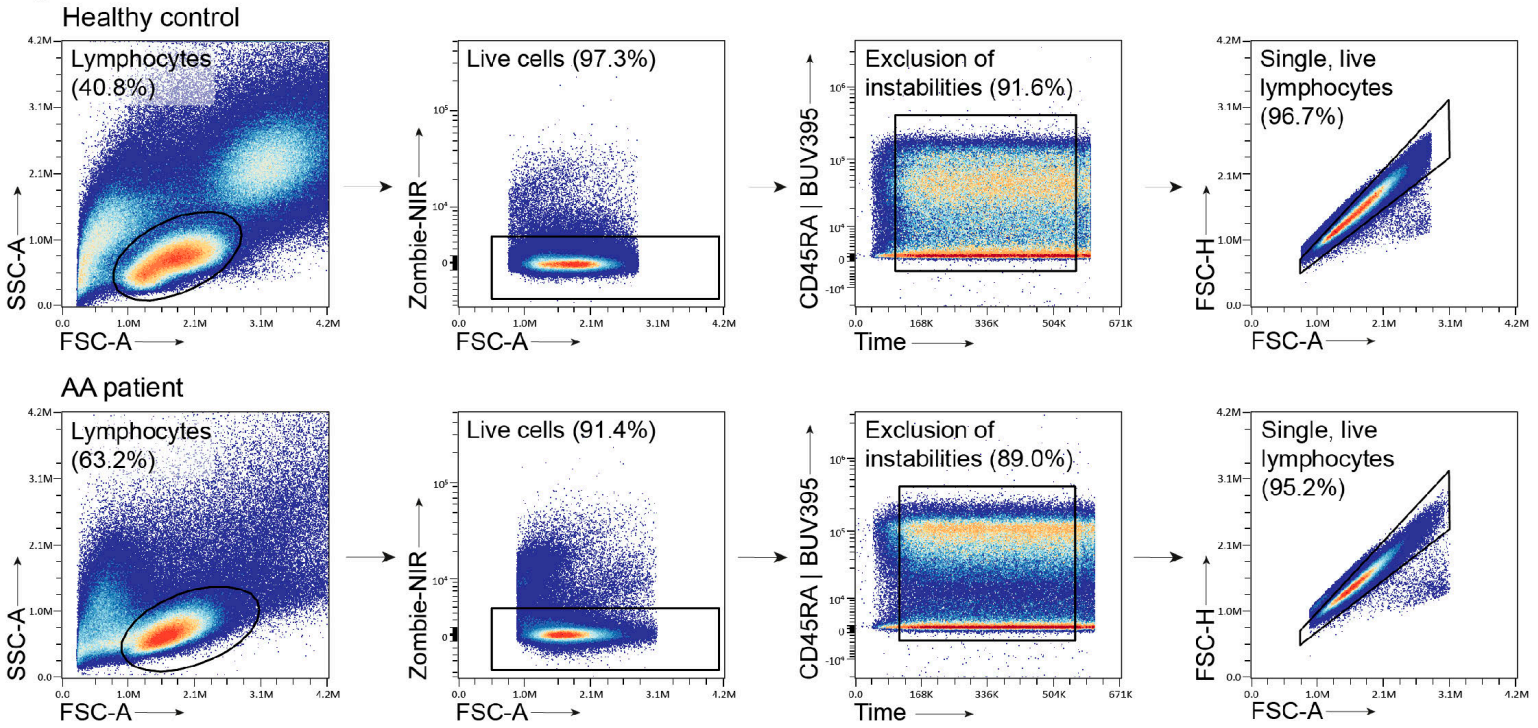


**Figure S3. Gating strategy for selection of single, live lymphocytes from spectral flow cytometry data.** Lymphocytes were gated in OMIQ based on the forward and side scatter (panel 1). Next, live cells were identified by selecting cells negative for Zombie-NIR (panel 2), and acquisition instabilities were removed by excluding events recorded at the beginning or end of each measurement (panel 3). Finally, doublets were excluded using the forward scatter height (FSC-H) and forward scatter area (FSC-A) parameters (panel 4). Data for a representative healthy control and aplastic anemia patient are shown. Single, live lymphocytes gated in panel 4 were selected for downstream analyses.

**Figure S4**

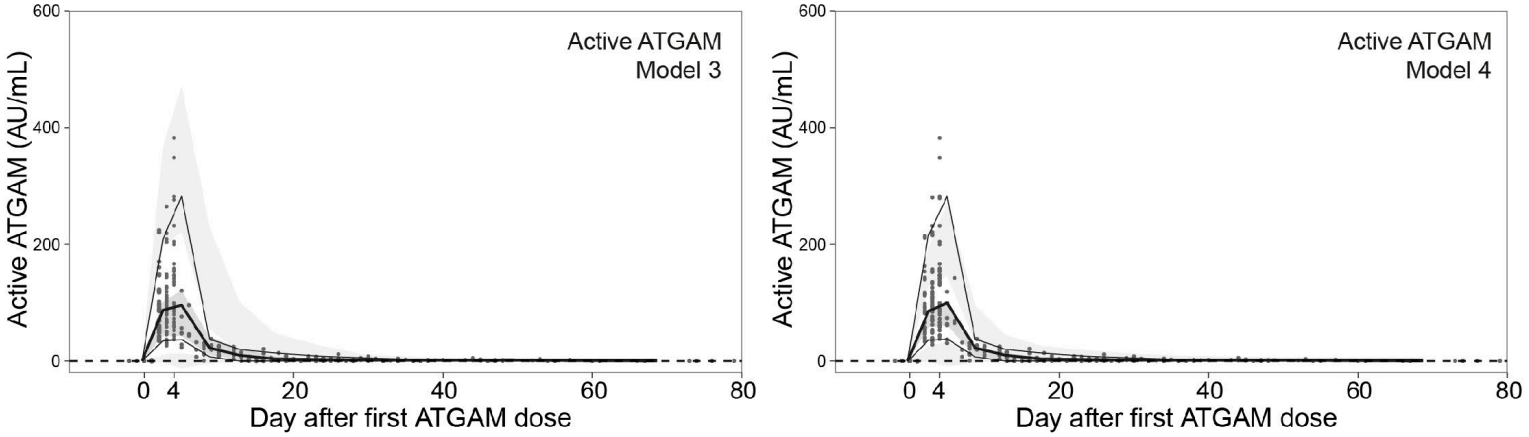


**Figure S4. Visual predictive checks for population pharmacokinetic model 3 and model 4 for active ATGAM.** Prediction-corrected visual predictive check (VPC) for the final model for active ATGAM. Black lines represent the predicted active ATGAM concentrations at the 95th, 50th, and 5th percentiles. Shaded light gray areas indicate the 95% confidence intervals for the predicted 5th and 95th percentiles, while the dark gray shaded area represents the 95% confidence interval for the predicted 50th percentile. Observed active ATGAM concentrations in all 44 AA patients are shown by black dots.

**Figure S5**

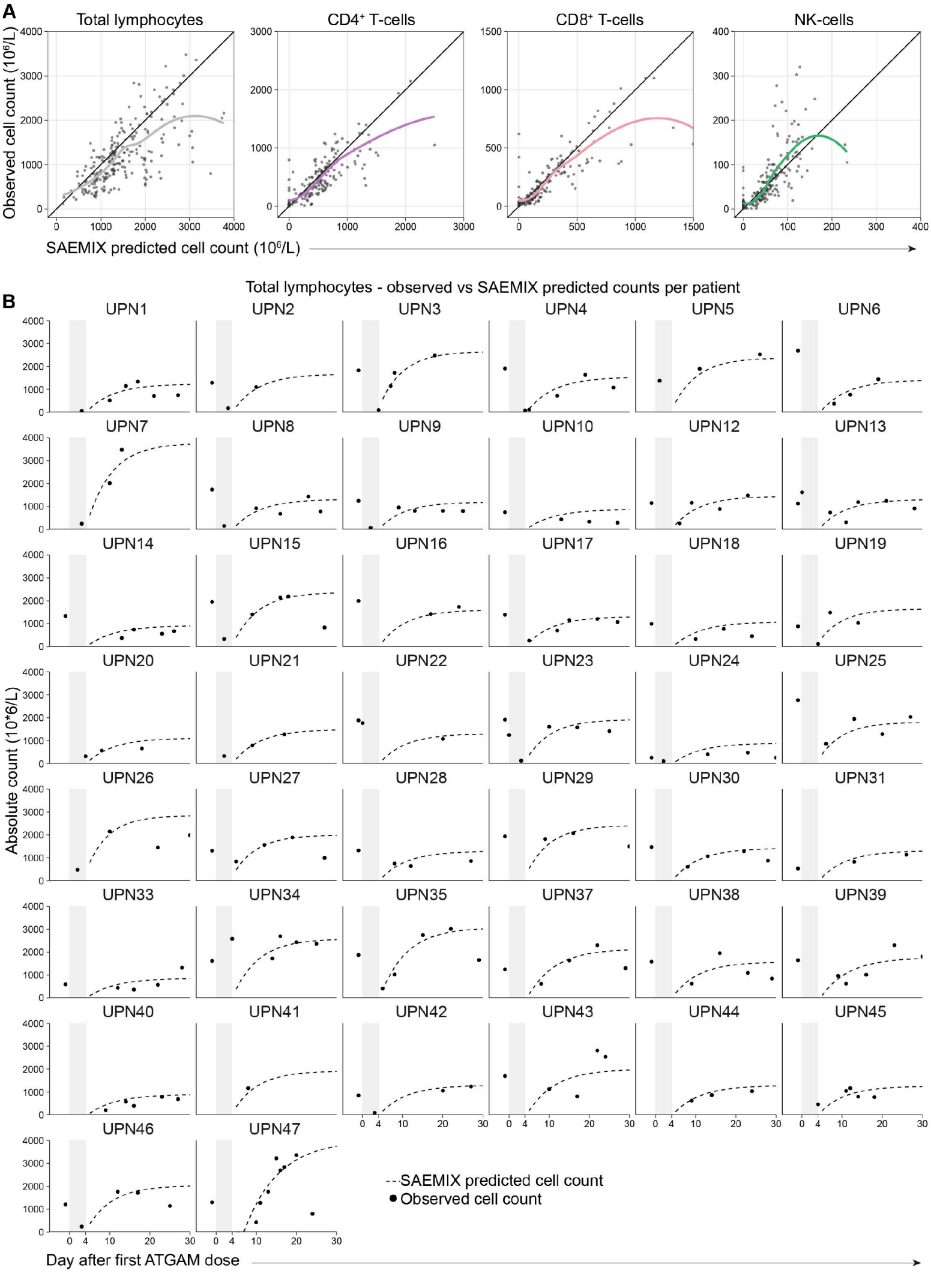
A
Total lymphocytes
CD4⁺ T-cells
CD8⁺ T-cells
NK-cells
Observed cell count (10⁶/L)
SAEMIX predicted cell count (10⁶/L)
B
Total lymphocytes - observed vs SAEMIX predicted counts per patient
UPN1
UPN2
UPN3
UPN4
UPN5
UPN6
UPN7
UPN8
UPN9
UPN10
UPN12
UPN13
UPN14
UPN15
UPN16
UPN17
UPN18
UPN19
UPN20
UPN21
UPN22
UPN23
UPN24
UPN25
UPN26
UPN27
UPN28
UPN29
UPN30
UPN31
UPN33
UPN34
UPN35
UPN37
UPN38
UPN39
UPN40
UPN41
UPN42
UPN43
UPN44
UPN45
UPN46
UPN47
Absolute count (10*6/L)
SAEMIX predicted cell count
Observed cell count
Day after first ATGAM dose

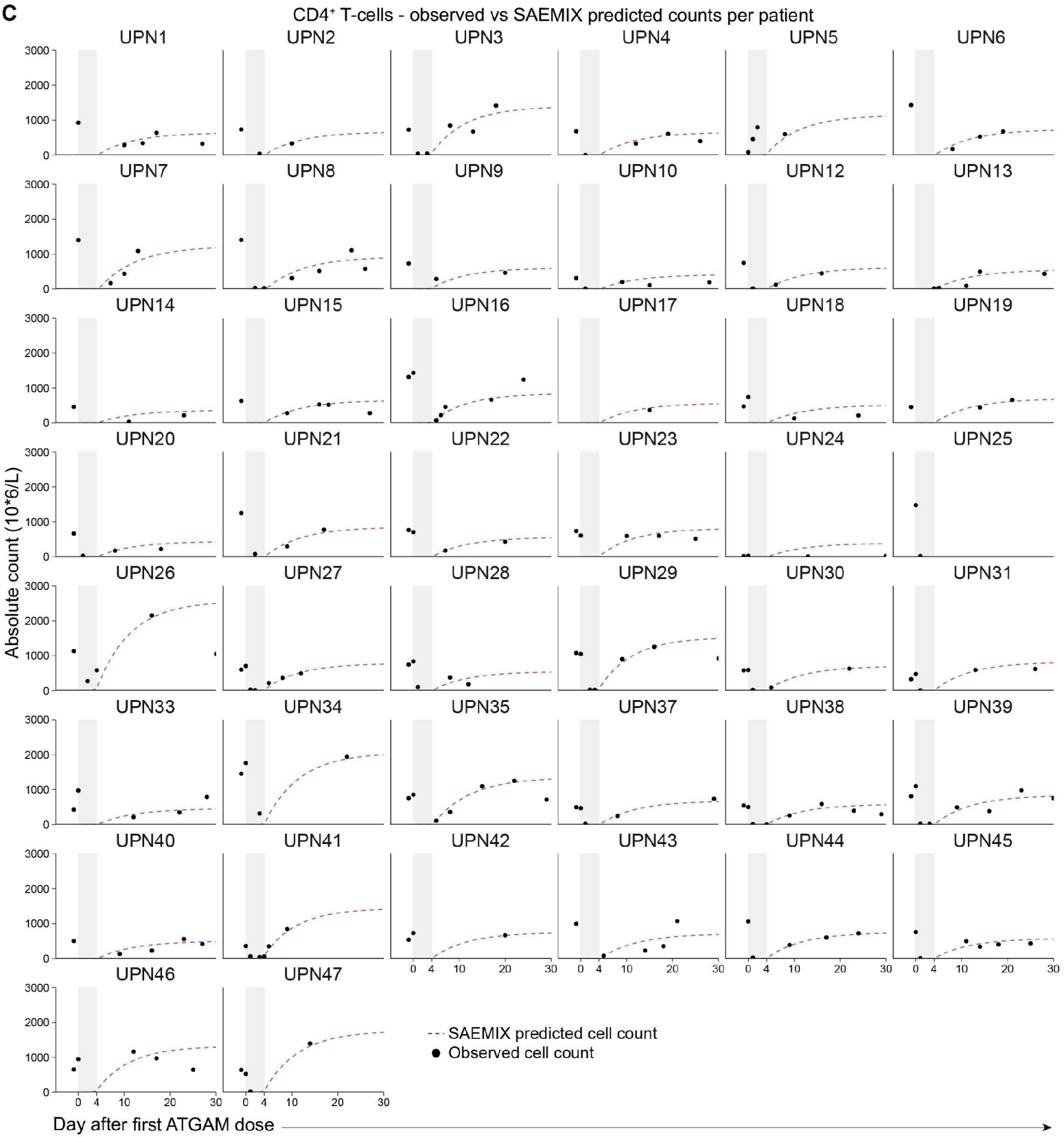
C
CD4⁺ T-cells - observed vs SAEMIX predicted counts per patient
UPN1
UPN2
UPN3
UPN4
UPN5
UPN6
UPN7
UPN8
UPN9
UPN10
UPN12
UPN13
UPN14
UPN15
UPN16
UPN17
UPN18
UPN19
UPN20
UPN21
UPN22
UPN23
UPN24
UPN25
UPN26
UPN27
UPN28
UPN29
UPN30
UPN31
UPN33
UPN34
UPN35
UPN37
UPN38
UPN39
UPN40
UPN41
UPN42
UPN43
UPN44
UPN45
UPN46
UPN47
Absolute count (10*6/L)
0
1000
2000
3000
0 4 10 20 30
SAEMIX predicted cell count
Observed cell count
Day after first ATGAM dose

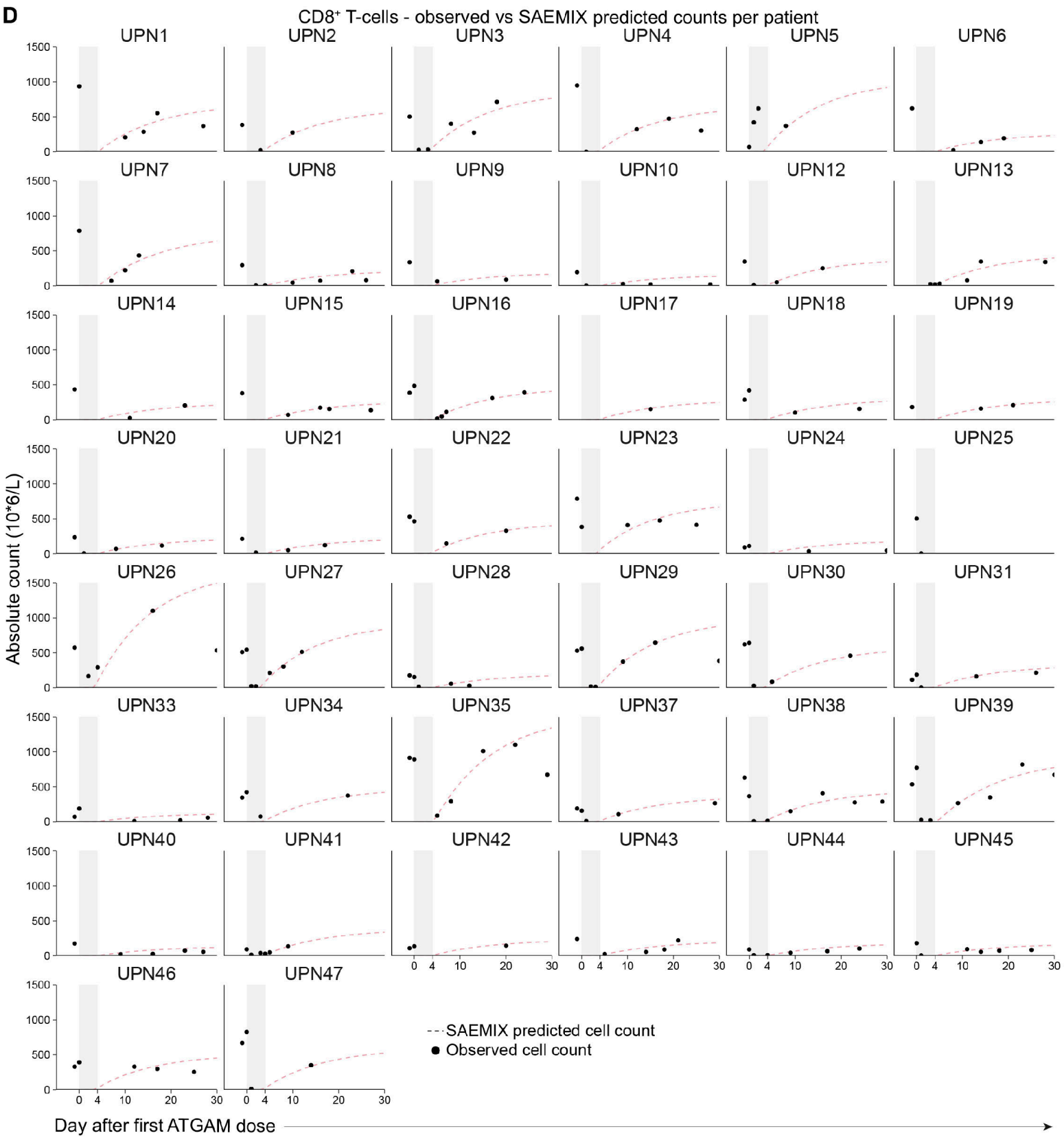
D
CD8⁺ T-cells - observed vs SAEMIX predicted counts per patient
UPN1
UPN2
UPN3
UPN4
UPN5
UPN6
UPN7
UPN8
UPN9
UPN10
UPN12
UPN13
UPN14
UPN15
UPN16
UPN17
UPN18
UPN19
UPN20
UPN21
UPN22
UPN23
UPN24
UPN25
UPN26
UPN27
UPN28
UPN29
UPN30
UPN31
UPN33
UPN34
UPN35
UPN37
UPN38
UPN39
UPN40
UPN41
UPN42
UPN43
UPN44
UPN45
UPN46
UPN47
Absolute count (10*6/L)
0
500
1000
1500
0 4 10 20 30
SAEMIX predicted cell count
Observed cell count
Day after first ATGAM dose

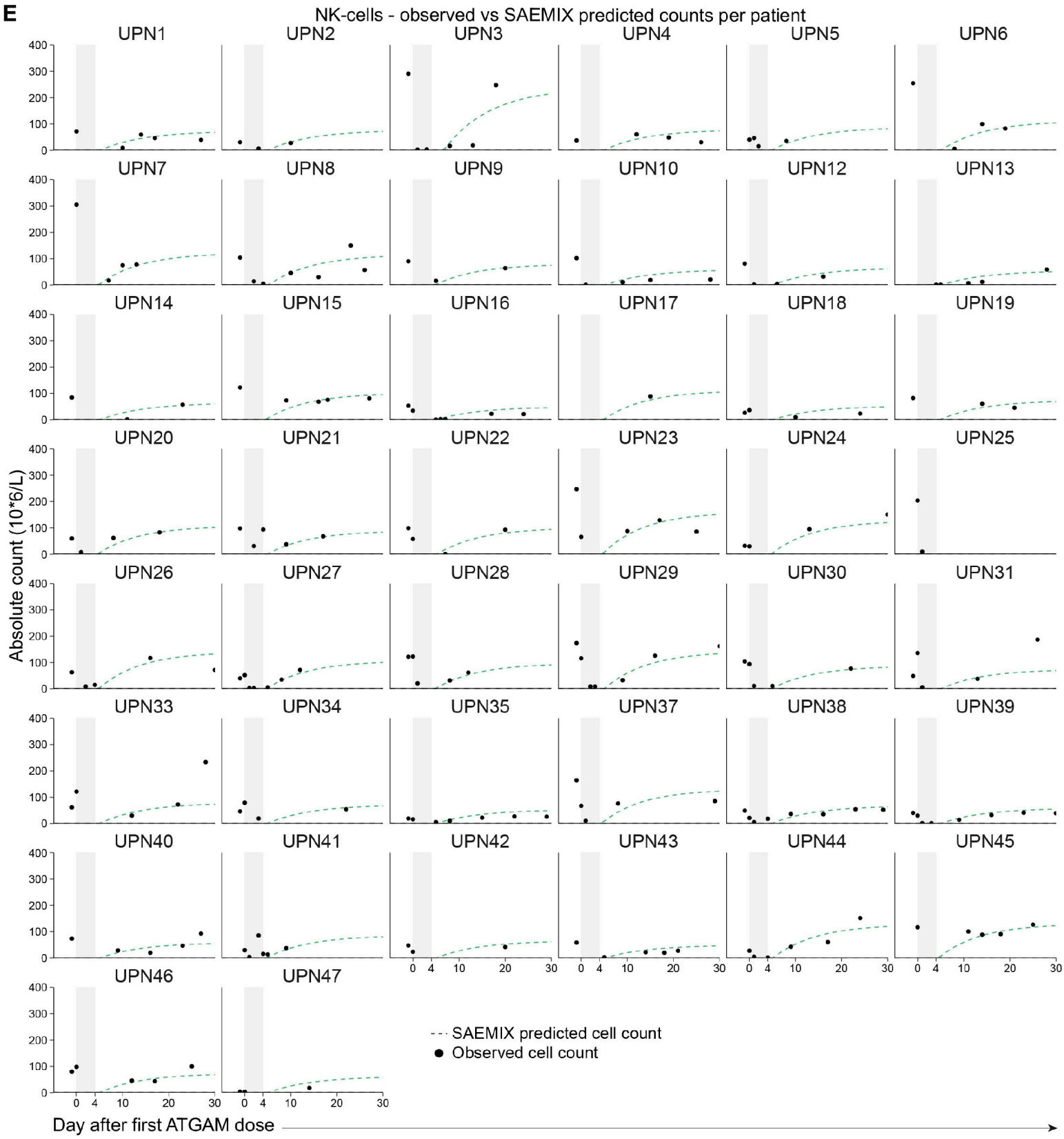


**Figure S5. Observed versus predicted immune reconstitution data. [A]** Observed versus SAEMIX-predicted total lymphocyte, CD4$^{+}$ T-cell, CD8$^{+}$ T-cell and NK-cell counts shown for all patients. The trend between observed and predicted counts are shown using loess regression. **[B-D]** Observed versus SAEMIX-predicted total lymphocyte **[B]**, CD4$^{+}$ T-cell **[C]**, CD8$^{+}$ T-cell **[D]** and NK-cell **[E]** counts per patient. Dots in present observed lymphocyte counts; dotted lines present predictions.

**Figure S6**

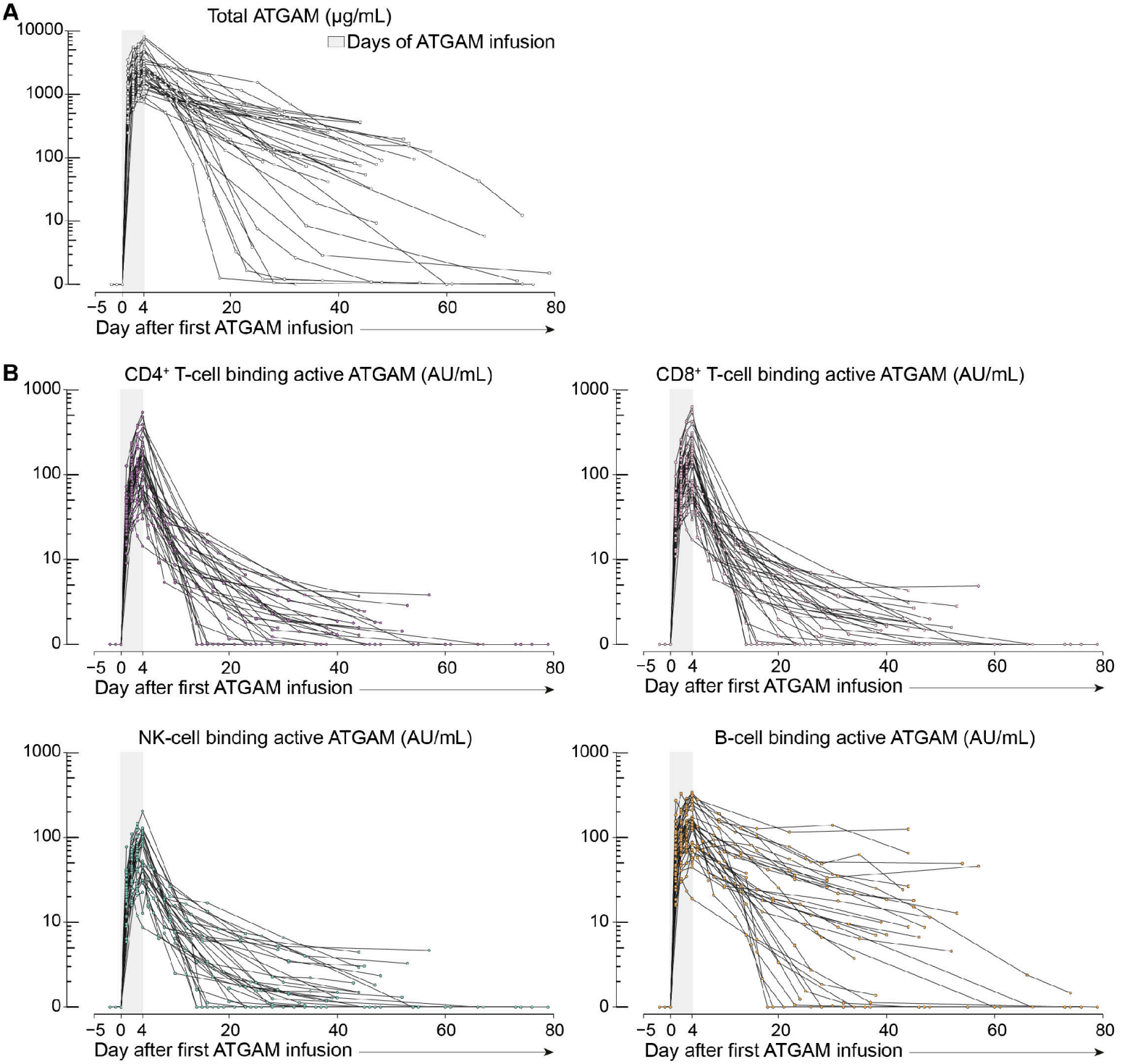


**Figure S6. Concentration-time profile of total ATGAM and lineage-binding active ATGAM in patient plasma. [A]** Measured total ATGAM, or **[B]** measured $CD4^+$ T-cell-binding active ATGAM, $CD8^+$ T-cell-binding active ATGAM, $CD19^+$ B-cell-binding active ATGAM, and NK-cell binding active ATGAM concentrations in patient plasma (in µg/mL or arbitrary units/mL; n=44 patients) over time before, during and after ATGAM infusion on days 0-4, shown on a logarithmic scale.

**Figure S7**

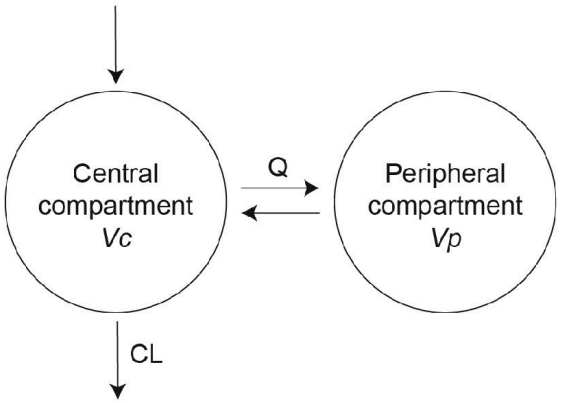


**Figure S7. Population pharmacokinetic model overview.** A two-compartment population pharmacokinetic model best described the total and active ATGAM concentration-time data. CL: linear clearance, Q: intercompartmental clearance between central compartment with volume Vc, and peripheral compartment with volume Vp.

**Figure S8**

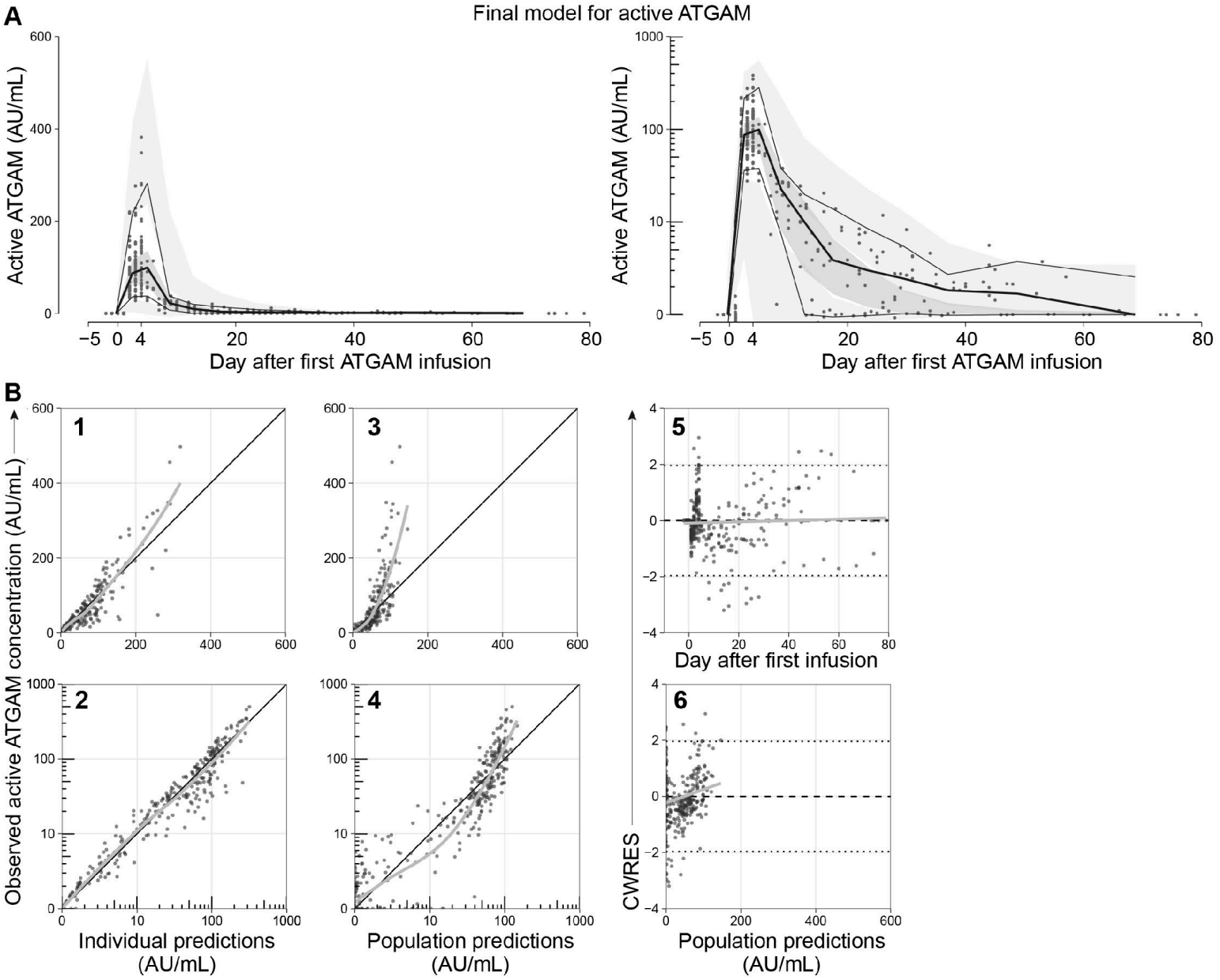


**Figure S8. Prediction-corrected visual predictive check and goodness of fit plots for the final pharmacokinetic model for active ATGAM. [A]** Prediction-corrected visual predictive check (VPC) for the final model for active ATGAM. Black lines represent the predicted active ATGAM concentrations at the 95th, 50th, and 5th percentiles. Shaded light gray areas indicate the 95% confidence intervals for the predicted 5th and 95th percentiles, while the dark gray shaded area represents the 95% confidence interval for the predicted 50th percentile. Observed active ATGAM concentrations in all 44 AA patients are shown by black dots. VPC is shown on a linear (left) or a logarithmic (right) scale. **[B]** Goodness of fit plots for the final model for active ATGAM. Observed versus individual predicted (IPRED) active ATGAM concentrations on a linear (1) and logarithmic (2) scale; observed versus population predicted (PRED) active ATGAM concentrations on a linear (3) and logarithmic (4) scale; conditional weighted residuals (CWRES) versus time after ATGAM infusion on days 0-4 (5); conditional weighted residuals (CWRES) versus population predicted active ATGAM concentrations (6). Dotted lines in (5) and (6) present the +/- 1.96 ranges of CWRES (95% confidence interval), which should include 95% of the CWRES values.

**Figure S9**

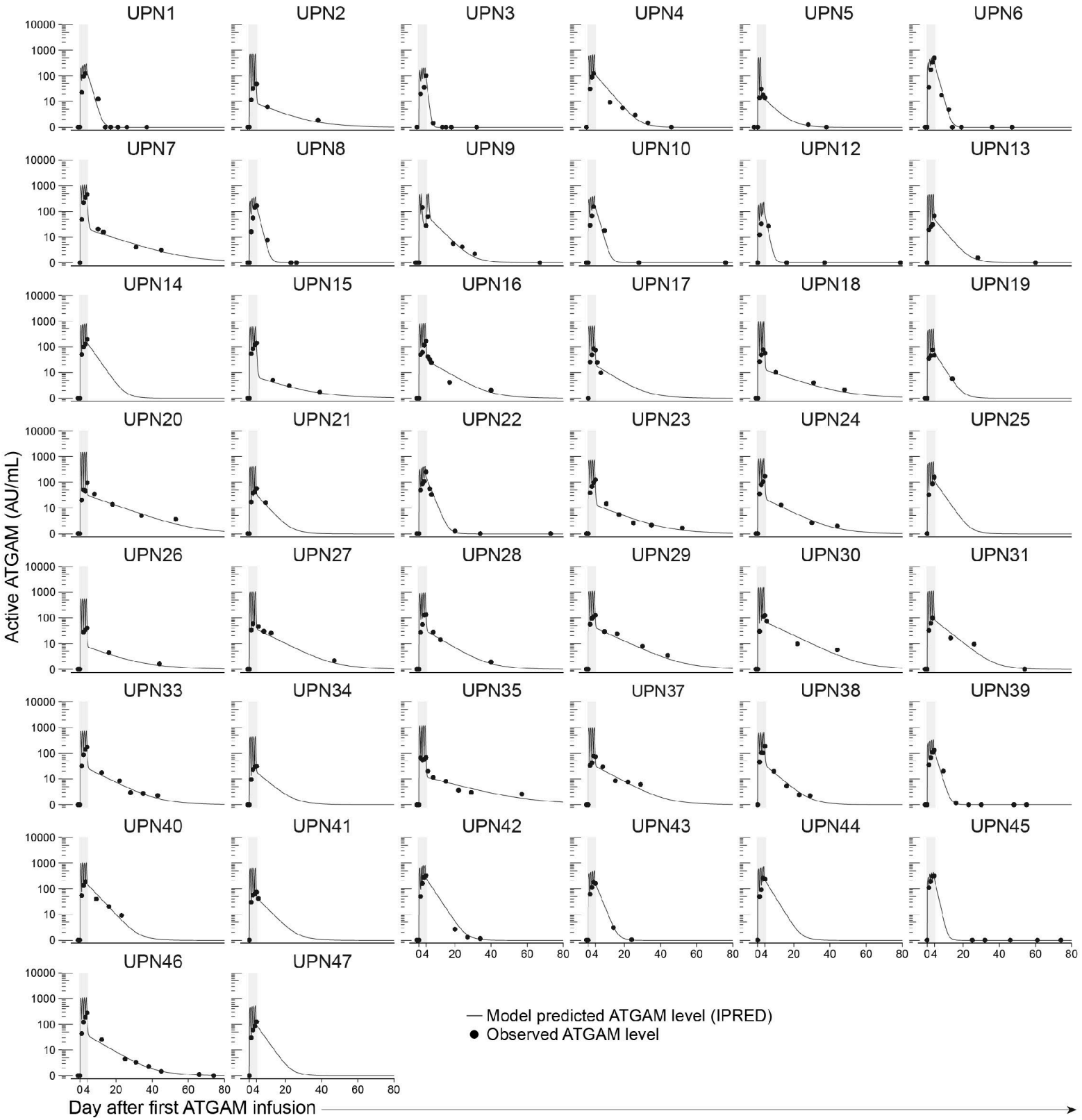


**Figure S9. Observed versus model-predicted active ATGAM concentrations per patient.** Observed active ATGAM concentrations are shown by black dots, while modelled active ATGAM concentrations in time are shown using black lines. Data are presented on a logarithmic axis.

**Figure S10**

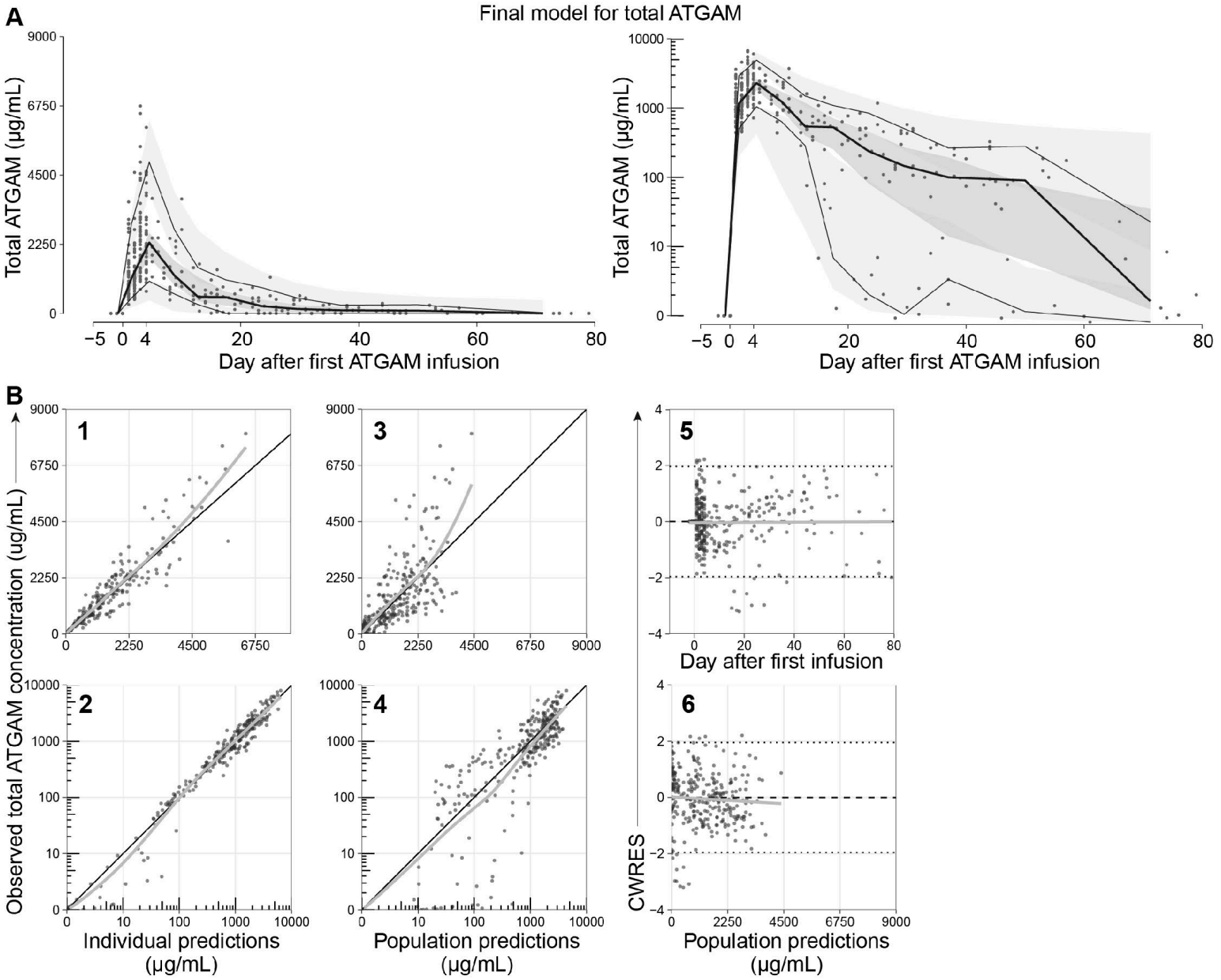


**Figure S10. Prediction-corrected visual predictive check and goodness of fit plots for the final pharmacokinetic model for total ATGAM. [A]** Prediction-corrected visual predictive check (VPC) for the final model for total ATGAM. Black lines represent the predicted total ATGAM concentrations at the 95th, 50th, and 5th percentiles. Shaded light gray areas indicate the 95% confidence intervals for the predicted 5th and 95th percentiles, while the dark gray shaded area represents the 95% confidence interval for the predicted 50th percentile. Observed total ATGAM concentrations in all 44 AA patients are shown by black dots. VPC is shown on a linear (left) or a logarithmic (right) scale. **[B]** Goodness of fit plots for the final model for total ATGAM. Observed versus individual predicted (IPRED) total ATGAM concentrations on a linear (1) and logarithmic (2) scale; observed versus population predicted (PRED) total ATGAM concentrations on a linear (3) and logarithmic (4) scale; conditional weighted residuals (CWRES) versus time after ATGAM infusion on days 0-4 (5); conditional weighted residuals (CWRES) versus population predicted total ATGAM concentrations (6). Dotted lines in (5) and (6) present the +/- 1.96 ranges of CWRES (95% confidence interval), which should include 95% of the CWRES values.

**Figure S11**

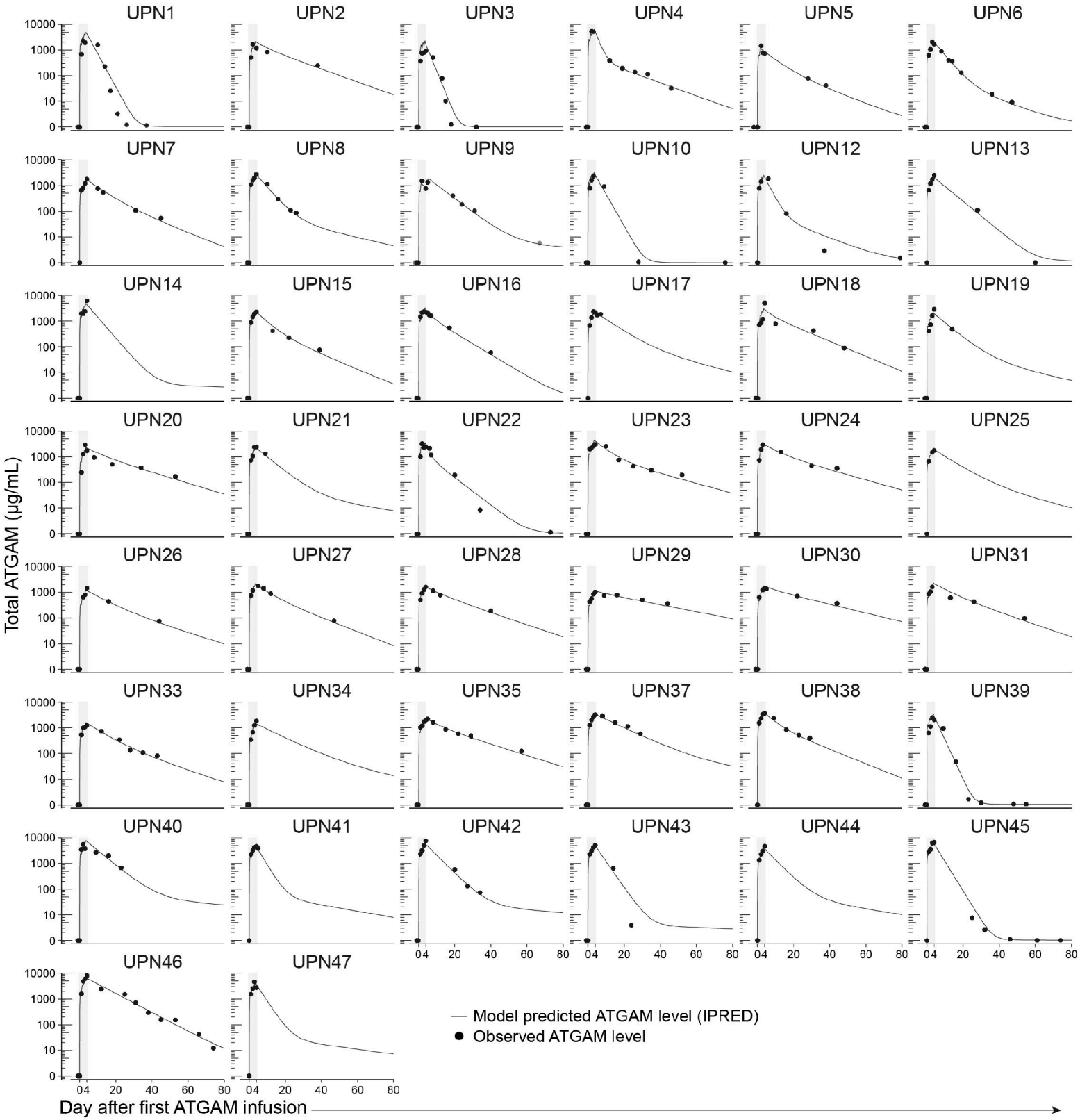


**Figure S11. Observed versus model-predicted total ATGAM concentrations per patient.** Observed total ATGAM concentrations are shown by black dots, while modelled total ATGAM concentrations in time are shown using black lines. Concentrations are presented on a logarithmic axis.

**Figure S12**

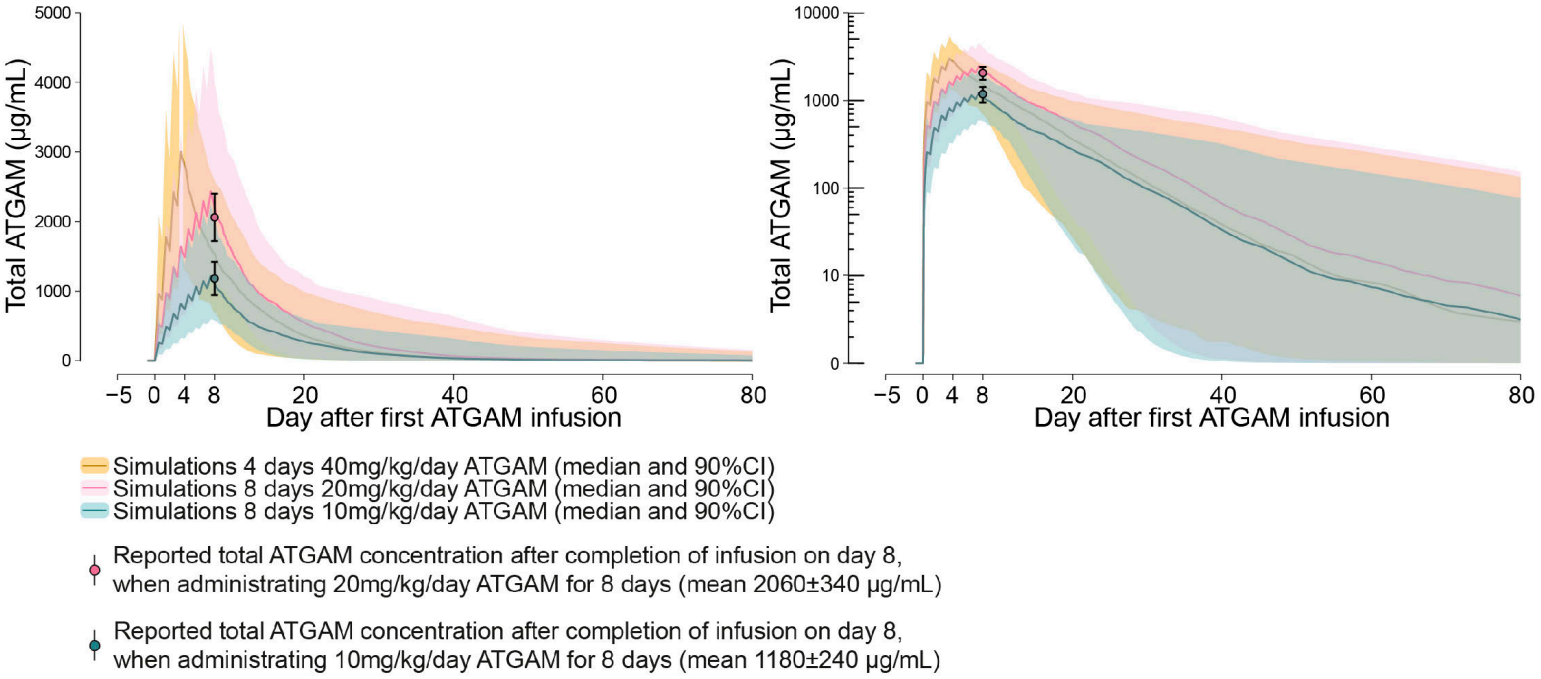


**Figure S12. Model simulations for alternative ATGAM dosing schemes.** The final pharmacokinetic model for total ATGAM was used to simulate the concentration-time profile of total ATGAM in time after the administration of 8 consecutive days 10mg/kg/day ATGAM, 8 consecutive days 20mg/kg/day ATGAM or 4 consecutive days 40mg/kg/day ATGAM. Lines and shaded areas represent the median and 90% confidence interval obtained from 100 simulations. Dots and error bars represent the mean and range of reported ATGAM peak concentrations following the completion of infusion on day 8 when ATGAM was administered at 10mg/kg/day ATGAM or 20mg/kg/day ATGAM for 8 consecutive days (reported concentrations are described in the manufacturer's brochure by Pfizer).

**Figure S13**

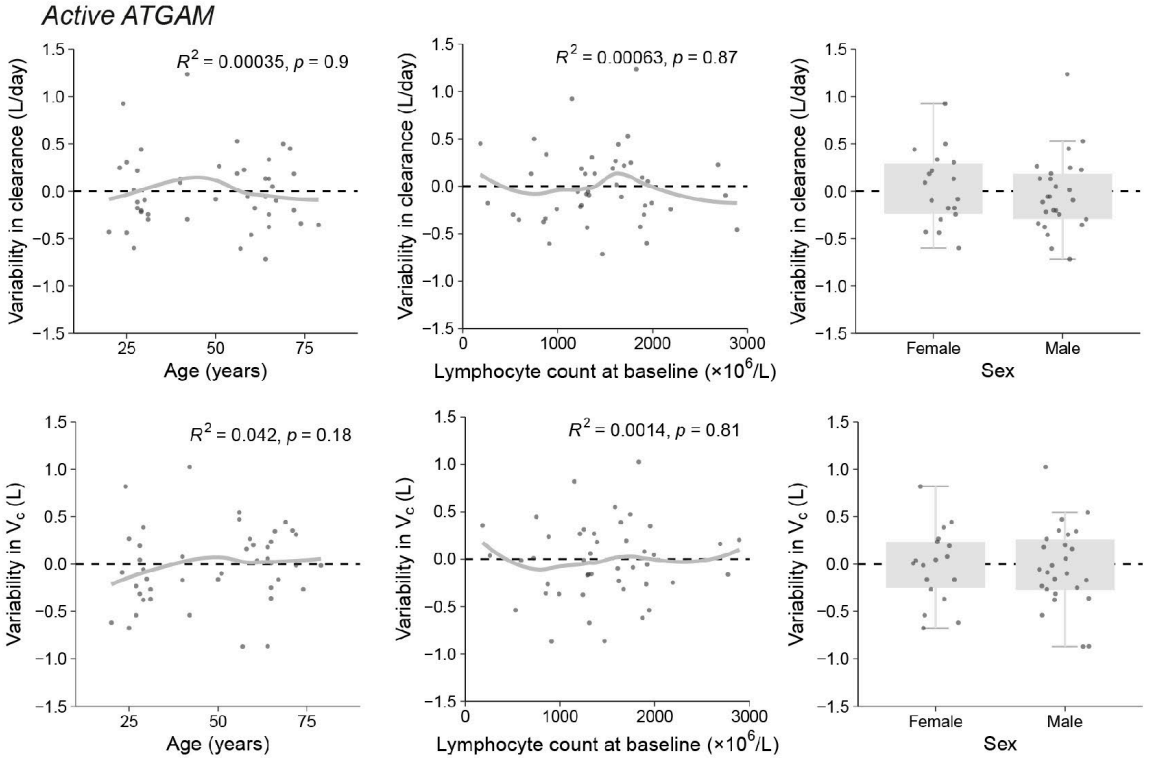


**Figure S13. Impact of demographical and clinical covariates on inter-individual variability in pharmacokinetic parameters.** Impact of age, lymphocytes pre-ATGAM and sex on inter-individual variability in clearance (row 1) and volume of distribution of the central compartment (row 2) of active ATGAM. Each dot represents a patient.

**Figure S14**

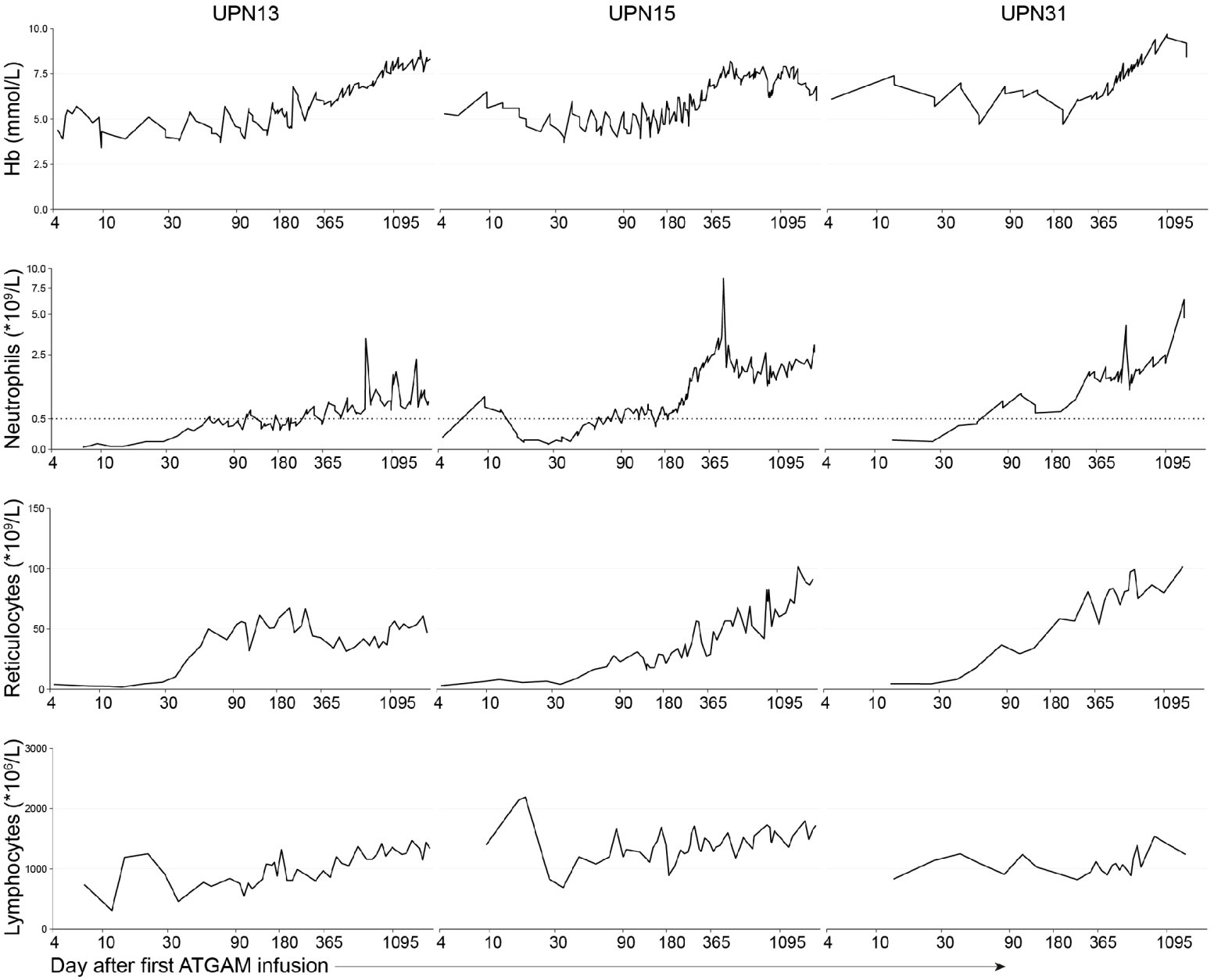


**Figure S14. Peripheral blood counts in time after start of ATGAM-based IST.** Hemoglobulin (Hb), neutrophil, reticulocyte and total lymphocyte counts in patients UPN13, UPN15 and UPN31 over time, up to 3.5 years after start of ATGAM-based IST.

**Figure S15**

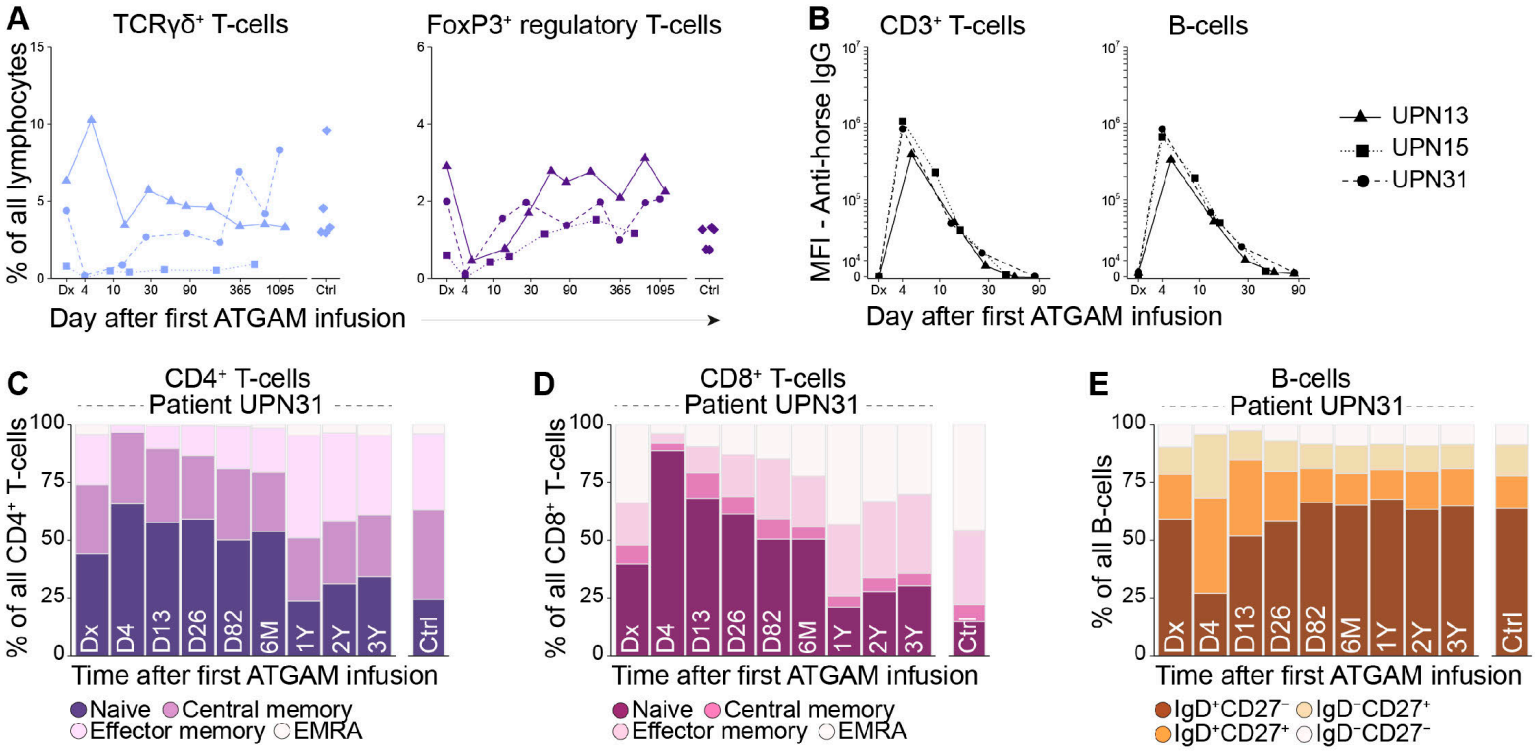


**Figure S15. Lymphocyte compartment pre- and over time post-ATGAM. [A]** Frequencies of major lymphoid lineages, shown as a percentage of all single, live lymphocytes per time point. Each line represents an individual patient. **[B]** Presence of ATGAM on the cell surface of T-cells (right) and B-cells (left), quantified over time using the mean fluorescence intensity of the Alexa Fluor 488-conjugated anti-horse IgG antibody. Each line represents an individual patient. **[C-E]** Bar plots quantifying the frequencies of subpopulations identified within the CD4⁺ T-cell, CD8⁺ T-cell and B-cell compartments from the representatitive patient UPN31. Flow cytometry plots are shown in Figure 4.

**Figure S16**

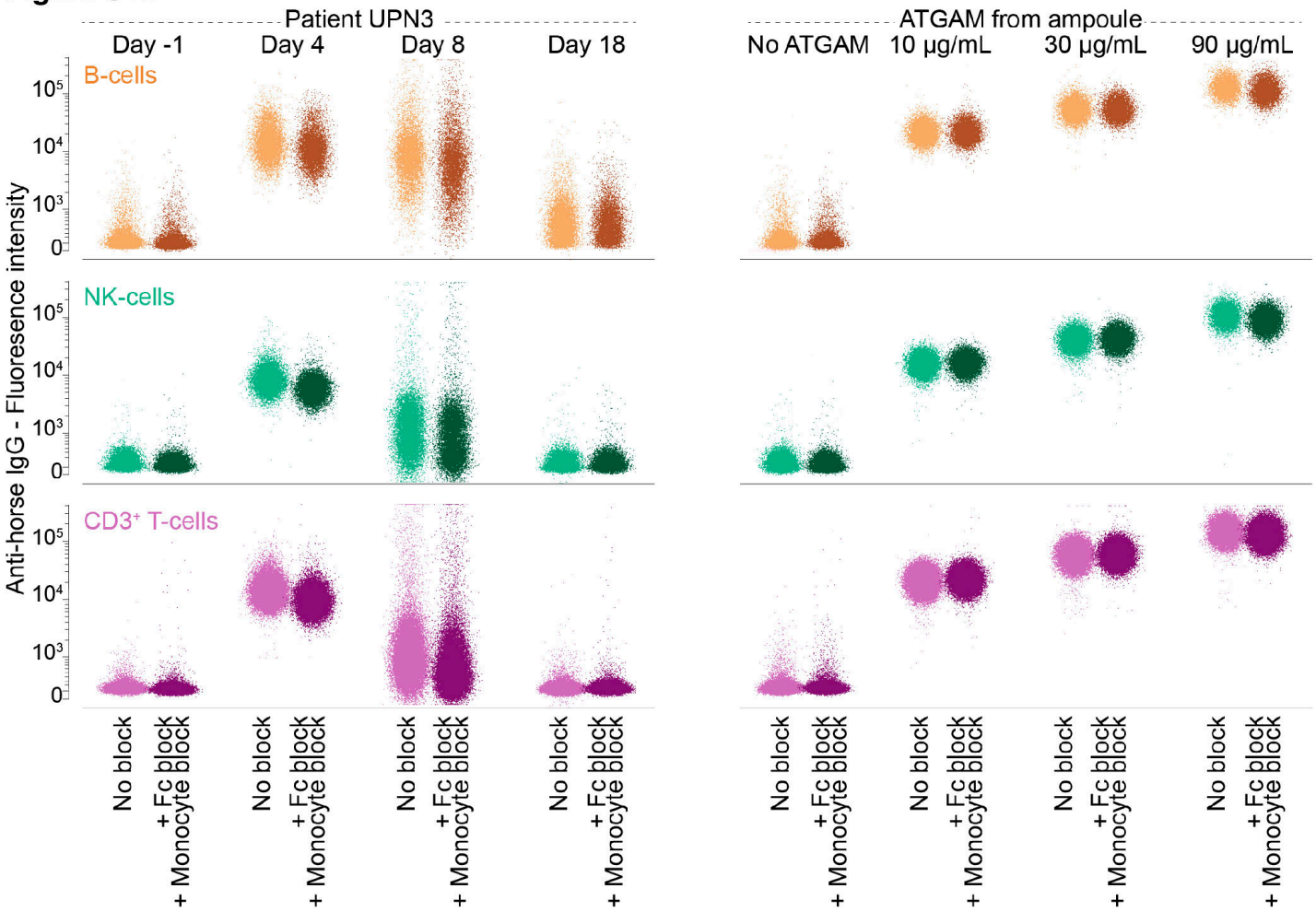


**Figure S16. Impact of Fc-receptor blockade on ATGAM binding to lymphoid lineages.** PBMCs from a healthy donor were pre-incubated without or with Fc-receptor block (Invitrogen, cat 14-9161-73) and monocyte block (Biolegend, cat 426103) for 30 minutes. Subsequently, cells were washed, co-incubated with undiluted plasma samples collected pre- and post-ATGAM infusion from patient LUMC3 (right), or known ATGAM concentrations (right), and stained as described in the methods section (see 'Quantification of active ATGAM concentrations').

**Figure S17**

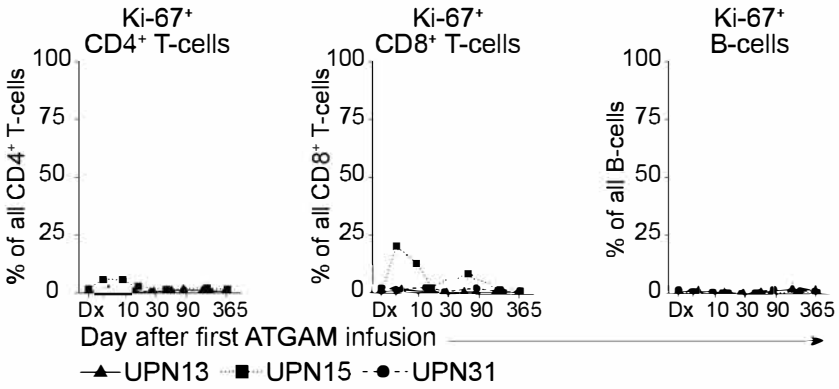


**Figure S17. Proliferating CD4+ T-cells, CD8+ T-cells and B-cells after start of ATGAM-based IST.** Ki-67+ cells were gated within the CD4+ T-cell, CD8+ T-cell and B-cell compartments. Data are shown for patients UPN13, UPN15 and UPN31.